ACS OMEGA

http://pubs.acs.org/journal/acsodf

Article

Tunable Anticorrosive Effects of Newly Synthesized Benzothiazole Azo Dyes by Potassium Iodide Synergism for Carbon Steel in 1 M HCl: Combined Experimental and Theoretical Studies

Mahmoud M. Youssif,* Marwa N. El-Nahass,* Tarek A. Fayed, Hosny A. El-Daly, Mohammed M. El-Gamil, and Ahmed M. Eldesoky

Cite This: *ACS Omega* 2023, 8, 28314−28332

Read Online

ACCESS | Metrics & More | Article Recommendations | Supporting Information

ABSTRACT: Herein, we synthesized three novel benzothiazole azo dyes, including 4-chloro-2-(4-methyl-benzothiazol-2-ylazo)-phenol (CMBTAP), 1-(6-chloro-benzothiazol-2-ylazo)-naphthalen-2-ol (CBAN), and 2-(6-chloro-benzothiazol-2-ylazo)-4-methyl-phenol (CBAMP), and investigated their corrosion inhibition effect on carbon steel. The dyes were characterized by Fourier transform infrared spectroscopy, ^{1}H nuclear magnetic resonance (NMR), ^{13}C NMR, and mass spectroscopy. Weight loss, electrochemical impedance spectroscopy, and potentiodynamic polarization measurements were performed to investigate the corrosion inhibition effect of the dyes on carbon steel in a 1.0 M HCl solution. The synergistic effects of the dyes with potassium iodide (KI) were also investigated. The inhibition efficiency (IE%) was enhanced by increasing the dose of the dyes (1×10^{-5} to 2×10^{-4} M) and decreased as the temperature increased from 25 to 45 °C. The addition of KI to a 1.0 M HCl solution containing the dyes improved the performance and efficiency as iodide ions promoted the formation of inhibition films on the surface of carbon steel. The dyes are mixed-type inhibitors, according to Tafel polarization. Scanning electron microscopy and energy dispersive X-ray analysis were used to evaluate the surface morphology of carbon steel sheets. Quantum theory calculations were utilized to evaluate the relationship between the dyes' chemical structures and their inhibitory efficiency, which confirmed the experimental results. The calculations revealed that the dyes have low energy gap and Milliken and Fukui indices. Among all of the dyes, CMBTAP showed the highest adsorption energy. The corrosion IE was in the order CMBTAP > CBAMP > CBAN.

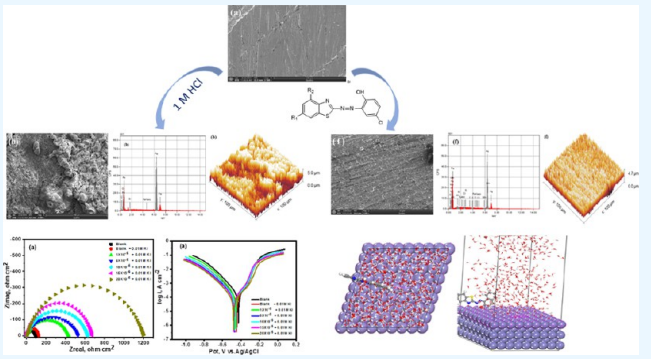

1. INTRODUCTION

Due to its outstanding mechanical properties at high temperatures, simplicity of production, and low cost, carbon steel plays a significant role in the petroleum industry for pipelines, tanks, ships, equipment, and other applications. Nevertheless, in acidic situations, it is vulnerable to corrosion. The two acids that are most frequently utilized in the industry are sulfuric acid and hydrochloric acid. They are employed to remove oxides produced by chemical processes in steel and oil refineries.[1−4] These acidic solutions can corrode metals over time. In aqueous environments, which are found in an array of challenging circumstances in oil and gas production, processing, and pipeline systems, the majority of metals are susceptible to corrosion.[5] The most cost-effective strategy is to slow the rate of corrosion because corrosion processes cannot be stopped. In recent years, organic compounds have been used extensively as corrosion inhibitors to prevent corrosion in metals.[6,7] Generally, the most effective organic inhibitors are heterocyclic compounds having π-electrons, heteroatoms, and aromatic rings. Heterocyclic azo dyes and Schiff bases have attracted attention as metal corrosion inhibitors in acidic conditions because they have higher inhibition efficiency (IE) than the comparable amines and aldehydes.[8−11] Comparatively to other organic inhibitors, azo dyes are more promising for the suppression of corrosion due to their molecular structures. According to several research studies,[12−14] the inhibition of corrosion by azo dyes is attributed to the formation of complexes between the metal and the nitrogen of the azo group binding at the electrode surface. Synergistic inhibition (synergism) is a successful method of improving the inhibitive force.[15] Halide ions increase the adsorption ability of organic cations in corrosive environments by establishing bridges between inhibitor cations and negatively

Received: April 1, 2023
Accepted: July 10, 2023
Published: July 27, 2023

Scheme 1. Synthetic Procedures and Chemical Structures of CMBTAP, CBAN, and CBAMP

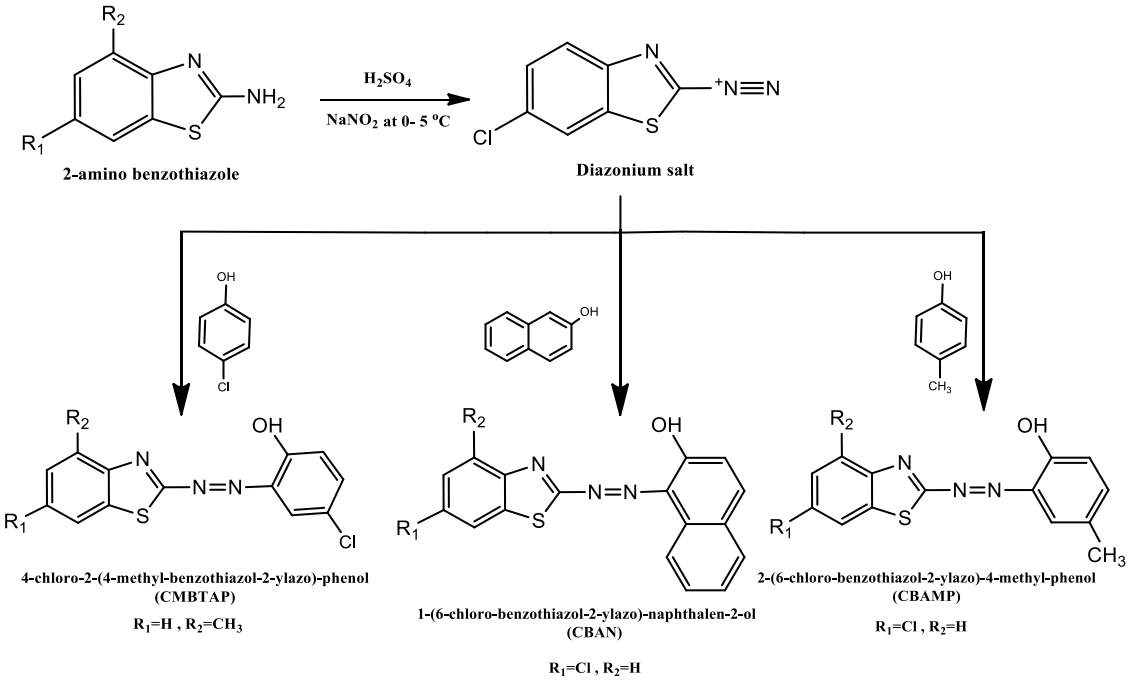

charged metal surfaces. The synergism of halide ions is in the order $I^- > Br^- > Cl^-$.[16] Owing to its relatively larger size and high polarizability, I^- is chemisorbed on metal surfaces and provides better synergistic effects.[17] Synergism is a successful approach to improve the inhibitory effect of inhibitors to reduce the dose of organic compounds and diversify the applications of inhibitors in acidic environments.[18] The association between molecular structures and the chemical reactivity and selectivity of corrosion inhibition mechanisms must also be established, and this requires utilizing quantum chemical calculations. The effectiveness of a compound in a chemical reaction is related to its spatial and electronic molecular structures.[19] Furthermore, theoretical studies enable the preselection of organic compounds with the required structural features for chemical reactions.

In this study, we synthesized three novel azo dyes, including 4-chloro-2-(4-methyl-benzothiazol-2-ylazo)-phenol (CMBTAP), 1-(6-chloro-benzothiazol-2-ylazo)-naphthalen-2-ol (CBAN), and 2-(6-chloro-benzothiazol-2-ylazo)-4-methyl-phenol (CBAMP) (Scheme 1), and examined their corrosion inhibition effects on carbon steel. The adsorption efficiency was analyzed by weight-loss measurements, potentiodynamic polarization, and electrochemical impedance spectroscopy (EIS) in 1.0 M HCl solutions. The IE% was enhanced by the addition of iodide ions to small concentrations of azo dyes containing a corrosive solution. Quantum theoretical analysis revealed the correlation between the molecular structures of the dyes and their corrosion IE. The surface morphology of carbon steel was evaluated by scanning electron microscopy (SEM) and energy dispersive X-ray spectroscopy (EDX).

2. EXPERIMENTAL SECTION

2.1. Materials and Reagents. 2-Amino-4-methyl benzothiazole, 2-amino-6-chloro benzothiazole, 6-chloro phenol, *p*-cresol, and *β*-naphthol were purchased from Merck-Aldrich Chemicals and used as received. Sodium hydroxide, sodium nitrite, and sulfuric acid (98%) were purchased from Beijing Chemical Int. AR-grade hydrochloric acid (30%) was used for preparing the corrosive solutions. Seven identical carbon steel specimens were cut out from a carbon steel sheet with chemical composition (wt %): C (0.076), Mn (0.19), P (0.012), Si (0.026), Cr (0.05), Al (0.023), and Fe (balance). The surfaces of carbon steel samples and the working electrode were polished to mirror finish using different grades (400−1200) from grit emery papers and washed with deionized water.

2.2. Synthesis and Characterization of Investigated Benzothiazole Azo Dyes. The investigated azo dyes, 4-chloro-2-(4-methyl-benzothiazol-2-ylazo)-phenol (CMBTAP) 1-(6-chloro-benzothiazol-2-ylazo)-naphthalen-2-ol (CBAN), and 2-(6-chloro-benzothiazol-2-ylazo)-4-methyl-phenol (CBAMP) (Scheme 1), were synthesized following the procedures previously described by us[20] to yield brownish red, reddish brown, and orange solids of CMBTAP, CBAN, and CBAMP, respectively, which were dried and recrystallized from ethanol.

The molecular structure of the investigated dyes, CMBTAP, CBAN, and CBAMP, was confirmed by FT-IR, ^{1}H NMR, ^{13}C NMR, and mass spectroscopy. Both CBAN and CBAMP dyes have been characterized and discussed by us previously.[20] The FT-IR spectrum of CMBTAP showed sharp bands at vibrational frequencies (cm^{-1}): 1469 (C−S), 1597 (C−N), 1532 (C═N), 1534 (N═N), 3120 (Ar═CH), 2930 (aliphatic−CH_3 group), 760 (C−Cl), and a sharp band is observed at 3456 cm^{-1} corresponding to stretching vibrations of the −OH group; see Figure S1. The mass spectra showed a molecular ion peak at the required position, m/z = 304.5, which is equivalent to the molecular weight of the proposed compound; see Figure S2. ^{1}H NMR (DMSO-d_6, 400 MHZ, Figure S3) shows that δ (ppm) = 11.12 (s, 1H, OH), 6.8 (s, 1H, phenol), 6.95 (s, 1H, phenol), 7.15 (d, 1H, phenol), 7.42 (s, 1H, benzo), 7.33 (s, 1H, benzo), 7.9 (s, 1H,benzo), and 2.35 (s, 3H, CH_3). Figure S4 shows the ^{13}C NMR spectra using DMSO-d_6 as a solvent.

2.3. Solutions. In this investigation, the corrosive medium was 1.0 M HCl solution and prepared by dilution of 30% HCl with distilled water. Corrosion experiments were performed in

https://doi.org/10.1021/acsomega.3c02105
ACS Omega 2023, 8, 28314−28332

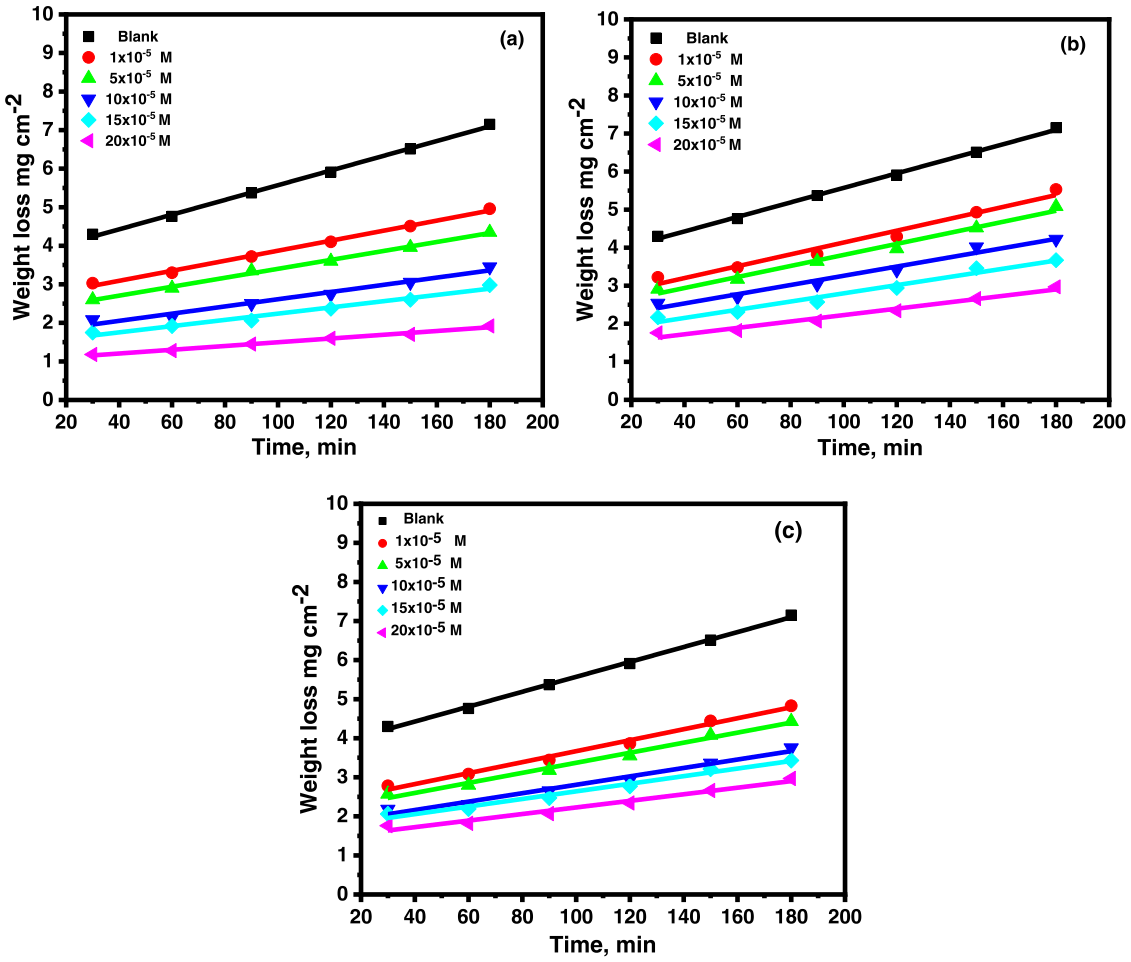

Figure 1. Weight-loss−time curves for the dissolution of carbon steel in 1.0 M HCl in the absence and presence of different concentrations of (a) CMBTAP, (b) CBAN, and (c) CBAMP at 25 °C.

1.0 M HCl solution in the absence and presence of various concentrations of synthesized azo dyes (1×10^{-5} to 2×10^{-4} M) and/or 0.5 M KI. Ethanol was used to prepare the stock solution of the investigated dyes (10^{-3} M). For each experiment, a freshly prepared solution was used under air atmosphere without stirring at 25 °C.

2.4. Weight-Loss Measurements. The weight-loss method, which is a practical and widespread method, was used to test the efficacy of corrosion inhibitors in acid solutions. In this method, the initial weight of thoroughly polished carbon steel samples (1 cm × 1 cm × 0.2 cm) was measured before immersion in 50 mL of 1.0 M HCl solution without and with different dosages of the investigated dyes CMBTAP, CBAN, and CBAMP. The measurements were performed at various temperatures (25−45 °C) for a total immersion time of 3 h using a thermostated water bath. After 30 min, sheets of carbon steel were removed from the solution, washed with distilled water, and then slowly dried with air before being weighed once more. The weight losses are given by

$$W = (m_1 - m_2) \tag{1}$$

where m_1 and m_2 are the weights of before and after exposure to the corrosive solution, respectively. The inhibition efficiency (% IE), the degree of surface coverage (θ), and corrosion rate (C) of the investigated dyes were calculated using eqs 2 and 3

$$\%\mathrm{IE} = \theta \times 100 = \left[1 - \left(\frac{W_{\mathrm{inh}}}{W_{\mathrm{free}}}\right)\right] \times 100 \tag{2}$$

$$\mathrm{CR} = \left[\frac{W}{A \times t}\right] \tag{3}$$

where W_{free} and W_{inh} are the weight losses per unit area in the absence and presence of inhibitors, respectively, A is the area of the carbon steel sheet in mg, and t is the period of immersion in minutes.

2.5. Electrochemical Measurements. CS Potentiostat/Galvanostat (electrochemical workstation CS350) with three derivative electrodes was used. The working electrode was carbon steel with 1 cm^2 surface area. Before each experiment, the electrode was abraded using emery sheets. After that, ethanol was used to clean the electrode using ultrasound before being rinsed with distilled water. All potentials were measured with reference to the Ag/AgCl electrode. A platinum plate with a surface area of 1 cm^2 served as the counter electrode. A steady-state open-circuit potential, OCP, was obtained by immersing the working electrode in the test solution for 30 min. In an atmosphere of air and at potentiodynamic conditions equivalent to 1 mV/s (sweep rate), Tafel polarization curves were recorded by combining different electrode potentials (−0.6 to 0.2 V) vs OCP. At 25 °C, all measurements were performed using a carbon steel electrode in 1.0 M HCl in the absence and presence

https://doi.org/10.1021/acsomega.3c02105
ACS Omega 2023, 8, 28314−28332

Table 1. Data of Weight-Loss Measurements for Carbon Steel in 1.0 M HCl Solution in the Absence and Presence of Different Concentrations of Investigated Inhibitors at 25 °C

inhibitor	conc. × 10^{-5} M	weight loss (mg cm^2)	CR (mg cm^{-2} min^{-1})	Θ	%IE
CMBTAP	blank	5.91	0.049		
	1	4.10	0.034	0.305	30.5
	5	3.60	0.03	0.3905	39.05
	10	2.74	0.022	0.535	53.5
	15	2.37	0.018	0.598	59.8
	20	1.73	0.014	0.707	70.7
CBAN	1	4.29	0.035	0.273	27.3
	5	3.97	0.033	0.328	32.8
	10	3.41	0.028	0.423	42.3
	15	2.94	0.024	0.502	50.2
	20	2.45	0.02	0.584	58.4
CBAMP	1	3.86	0.032	0.349	34.6
	5	3.55	0.029	0.399	39.9
	10	2.93	0.024	0.503	50.3
	15	2.77	0.023	0.531	53.1
	20	2.34	0.018	0.603	60.3

Table 2. Data of Weight-Loss Measurements for Carbon Steel in 1.0 M HCl Solution in the Absence and Presence of Different Concentrations of Investigated Inhibitors at Different Temperatures

		30 °C		35 °C		40 °C		45 °C	
inhibitor	conc. × 10^{-5} M	Θ	%IE	Θ	%IE	Θ	%IE	Θ	%IE
CMBTAP	1	0.265	26.5	0.229	22.9	0.208	20.8	0.162	16.2
	5	0.354	35.4	0.325	32.5	0.303	30.3	0.283	28.3
	10	0.503	50.3	0.475	47.5	0.463	46.3	0.426	42.6
	15	0.578	57.8	0.562	56.2	0.557	55.7	0.525	52.5
	20	0.689	68.9	0.673	67.3	0.661	66.1	0.636	63.6
CBAN	1	0.233	23.3	0.197	19.7	0.175	17.5	0.118	11.8
	5	0.292	29.2	0.262	26.2	0.241	24.1	0.221	22.1
	10	0.391	39.1	0.363	36.3	0.347	34.7	0.314	31.4
	15	0.478	47.8	0.461	46.1	0.451	45.1	0.429	42.9
	20	0.569	56.9	0.552	55.2	0.543	54.3	0.515	51.5
CBAMP	1	0.306	30.6	0.279	27.9	0.248	24.8	0.183	18.3
	5	0.362	36.2	0.334	33.4	0.312	31.2	0.291	29.1
	10	0.471	47.1	0.443	44.3	0.427	42.7	0.393	39.3
	15	0.508	50.8	0.501	50.1	0.49	49	0.498	49.8
	20	0.584	58.4	0.568	56.8	0.559	55.9	0.532	53.2

of various doses of the investigated inhibitors. The inhibition efficiency and surface coverage (Θ) were calculated from eq 4

$$\%IE = \theta \times 100 = \left[1 - \left(\frac{i_{corr(inh)}}{i_{corr(free)}}\right)\right] \times 100 \quad (4)$$

where $i_{corr(free)}$ and $i_{corr(inh)}$ are the corrosion current densities in the absence and presence of inhibitors, respectively.

Electrochemical impedance spectroscopy (EIS) measurements were performed using the identical cell that was used for polarization experiments. The EIS was carried out over a frequency range of 1 Hz to 100 kHz, with a signal-amplitude perturbation of 10 mV. The inhibition efficiency (%IE) and surface coverage (Θ) of the investigated compounds obtained were calculated from eq 5

$$\%IE = \theta \times 100 = \left[\left(\frac{R_{ct} - R^{o}_{ct}}{R_{ct}}\right)\right] \times 100 \quad (5)$$

where R°_{ct} and R_{ct} are the charge-transfer resistance values in the absence and presence of the inhibitor, respectively.

2.6. Surface Examinations Using Scanning Electron Microscopy (SEM) and Energy Dispersive X-ray (EDX) Spectroscopy. After retaining the carbon steel sheets for 24 h immersing in 1.0 M HCl solution in the absence and presence of higher concentrations of the investigated dyes, as well as with a mixture from dyes and 0.01 M KI solutions, the surface of carbon steel specimens was examined using a scanning electron microscope model: JEOL-JSM 6390.

2.7. Computational Study. The DMol^3 module of the Materials Studio programme (version 20.1 from BIOVIA Inc.) was used to perform density functional theory (DFT) calculations.[21,22] Numerical functions on an atom-centered grid, which are much more comprehensive than conventional Gaussian functions, are the atomic basis of the DMol^3 programme. Geometrical optimizations have been carried out using the double numerical with the polarization (DNP) basis set and the hybrid functional of Becke-3-exchange plus Lee–Yang–Parr correlation (B3LYP). The conductor-like screening model (COSMO)[23] was used to account for solvent effects (here, water, dielectric constant of 78.54) in order to achieve more reliable results.

https://doi.org/10.1021/acsomega.3c02105
ACS Omega 2023, 8, 28314−28332

The adsorption progress of CMBTAP, CBAN, and CBAMP on the iron surface is investigated using Monte Carlo simulations with Accelrys Inc.'s adsorption locator module.[24] We choose Fe(110) to simulate the adsorption process because, among the three types of Fe surfaces (110, 100, and 111), Fe(111) and Fe(100) have comparatively open structures, whereas Fe(110) is a density packed surface with the highest stabilization.[25,26] It was initially split from a bcc Fe crystal, then increased to a (8 × 8) supercell size, and then a 35 thickness vacuum slab was constructed above the Fe(110) plane. Using a simulated annealing task, the optimized inhibitor molecules were allowed to adsorb on the polished Fe(110) surface in order to reach an equilibrium configuration of the inhibitor/Fe(110) system. Lastly, we can determine the adsorption energy for the inhibitor/Fe(110) system configuration that is most stable. Each adsorption system also included 400H_2O, 5H_3O^+, and 5HCl molecules to simulate solvent effects. A forcefield method technological advance is the use of COMPASS (Condensed-phase Optimized Molecular Potentials for Atomistic Simulation Studies), which optimizes the structures of every system component.[27] It is the first ab-initio forcefield to predict chemical properties (structural, conformational, vibrational, etc.) and condensed-phase properties (equation of state, cohesive energies, etc.) for a wide range of chemical systems.

3. RESULTS AND DISCUSSION

3.1. Weight-Loss Measurements. Figure 1 shows the effect of the concentrations of CMBTAP, CBAN, and CBAMP on weight loss vs time of carbon steel at 25 °C. The weight loss of the carbon steel in the presence of the inhibitors increased linearly over time and was less than that attained in the absence of the inhibitors. The linearity shows that no insoluble surface film was created during the corrosion reaction, and the inhibitors were first adsorbed on the metal surfaces, separating them from the corrosive media and decreasing the metal dissolution and corrosion rate as the concentration increased (1×10^{-5} to 2×10^{-4} M).[28] Tables 1 and 2 show the calculated inhibition efficiencies (IE%) at various doses of inhibitors in 1.0 M HCl at various temperatures (25−45 °C). IE% increased with an increase in the inhibitor dose and decreased with temperature increase. This is explained by the increase in the number of inhibitor molecules that are adsorbed on the metal surface, and the promotion of inhibitor molecule desorption from the metal surface occurred at high temperatures. For the same inhibitor concentration (2×10^{-4} M), IE% increase in the following sequence: CMBTAP > CBAMP > CBAN.

3.2. Adsorption Isotherms. Basic information about corrosion inhibition mechanisms in electrochemical reactions can be provided in adsorption isotherms. Physical and chemical adsorption are two different types of interactions that occur when organic molecules adsorb on the surface of carbon steel. These interactions are affected by the chemical structure of the inhibitor, the type of electrolyte, and the charge and nature of the metal. The surface coverage θ of the metal surface by the adsorbed inhibitors was calculated from weight-loss measurements using eq 6. θ was evaluated for different inhibitor concentrations at 25 °C by fitting various isotherms, including Frumkin, Langmuir, Temkin, and Flory−Huggins isotherms. The Langmuir isotherm showed the best fit[29]

$$\frac{\theta}{1-\theta} = K_{ads} \times C \quad (6)$$

where C is the inhibitor concentration and K_{ads} the equilibrium constant of the adsorption process. Figure 2 shows a plot of $(\theta/1-\theta)$ against C for all concentrations of the inhibitors. A straight-

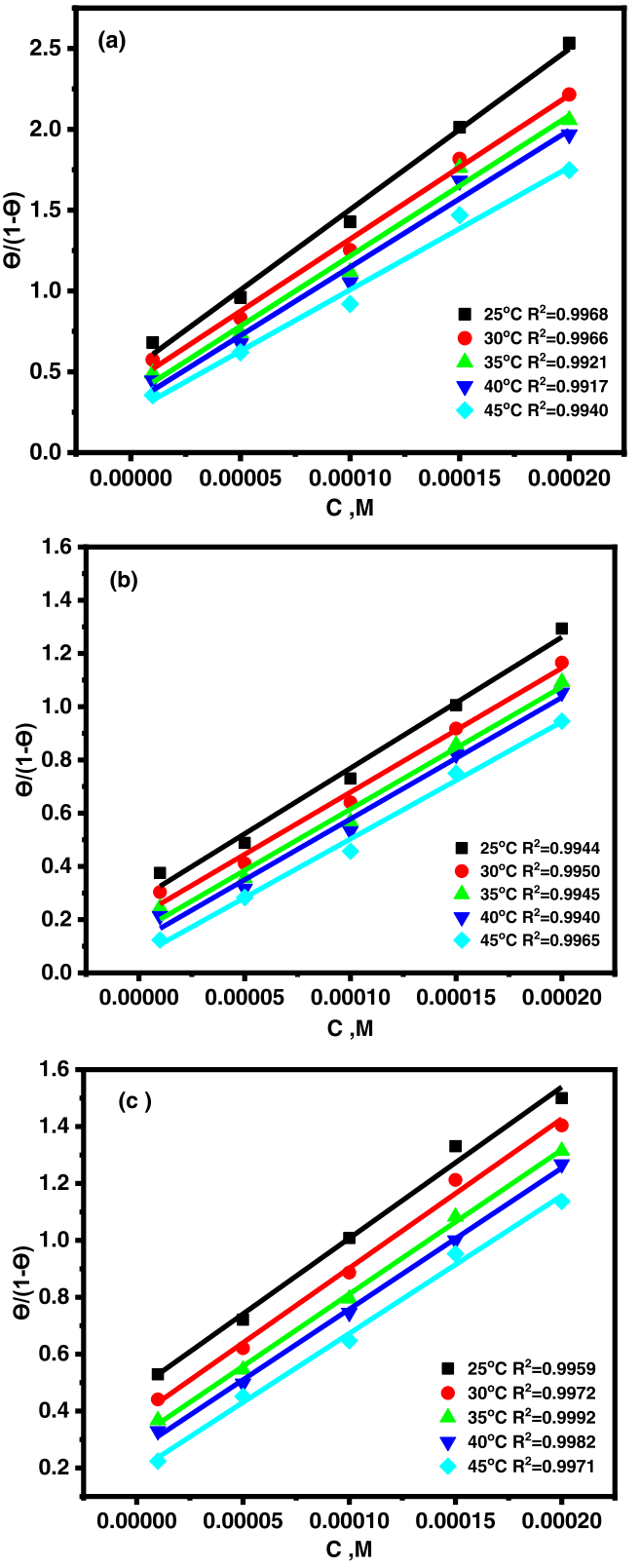

Figure 2. Langmuir adsorption isotherms of (a) CMBTAP, (b) CBAN, and (c) CBAMP on the carbon steel surface in 1.0 M HCl at different temperatures.

https://doi.org/10.1021/acsomega.3c02105
ACS Omega 2023, 8, 28314−28332

Table 3. Thermodynamic Parameters for the Adsorption of Inhibitors on the Carbon Steel Surface in 1.0 M HCl at Different Temperatures

inhibitor	temp. (K)	$K_{ads} \times 10^3$ M^{-1}	$-\Delta G^\circ_{ads}$ (kJ mol^{-1})	$-\Delta H^\circ_{ads}$ (kJ mol^{-1})	$-\Delta S^\circ_{ads}$ (J mol^{-1} k^{-1})
CMBTAP	298	9.94	32.73	4.06	96.2
	303	8.92	33.01		95.54
	308	8.68	33.5		95.58
	313	8.45	33.9		95.33
	318	7.58	34.2		94.77
CBAN	298	4.91	31	1.74	98.2
	303	4.70	31.4		97.8
	308	4.59	31.9		97.6
	313	4.52	32.4		97.3
	318	4.40	32.9		97.5
CBAMP	298	5.32	31.2	1.70	99.1
	303	5.25	31.6		98.2
	308	5.07	32.2		99.3
	313	4.96	32.8		99.4
	318	4.85	33.1		98.8

line relationship was obtained in all cases with correlation coefficients (R^2) of greater than 0.994. The standard free energy of adsorption ΔG°_{ads} was calculated using eq 7

$$K_{ads} = \frac{1}{55.5} e^{(-\Delta G^0_{ads}/RT)} \quad (7)$$

where 55.5 is the concentration of water in the solution in mole per liter, R the universal gas constant, and T the absolute temperature. The slope's deviation from unity shows that there were interactions between adsorbed species on the metal surface as well as changes in adsorption heat with increasing surface coverage,[30,31] which was ignored in the derivation of the Langmuir isotherm. The negative ΔG°_{ads} for CMBTAP, CBAN, and CBAMP (Table 3) indicate the spontaneity of the adsorption process and the stability of the adsorbed layer on the carbon steel surface.[32] ΔG°_{ads} of −20 kJ mol^{-1} or lesser enables physisorption, whereas that around −40 kJ mol^{-1} or higher promotes chemisorption due to charge sharing or transfer from the inhibitor molecules to the metal surface to form covalent bonds.[33,34] The obtained ΔG°_{ads} for CMBTAP, CBAN, and CBAMP are −31.2 to −33.1, −31.1 to −32.9, and −32.7 to −34.2 kJ mol^{-1}, respectively. This indicates that the adsorption mechanisms of the inhibitors on carbon steel in a 1.0 M HCl solution are physisorption and chemisorption (mixed one).

The adsorption heat was calculated according to Van't Hoff equation [eq 8][35]

$$\ln K = \left(\frac{-\Delta G^\circ_{ads}}{RT}\right) + \text{const} \quad (8)$$

Figure S5 shows a plot of log K_{ads} vs $1/T$ for the dissolution of carbon steel in 1.0 M HCl in the presence of inhibitors. The ΔH°_{ads} values are negative, as shown in Table 3, indicating that the adsorption is an exothermic process.[36] Additionally, the standard adsorption entropy ΔS°_{ads} was calculated using eq 9

$$\Delta S^\circ_{ads} = \left(\frac{\Delta H^\circ_{ads} - \Delta G^\circ_{ads}}{T}\right) \quad (9)$$

Negative ΔS°_{ads} values were obtained as shown in Table 3, indicating that the adsorption is an exothermic process and accompanied by a decrease in entropy. This is attributed to the adsorption of organic inhibitor molecules from the aqueous solution. This can be regarded as a quasi-substitution process between the organic compound in the aqueous phase [Org(sol)] and water molecules at the electrode surface [H_2O(ads)].[37,38] In this circumstance, adsorption of inhibitors is accompanied by desorption of water molecules from the electrode surface. However, the adsorption of the solvent is assumed to be endothermic and associated with an increase in entropy, and the adsorption of the inhibitor is supposed to be exothermic and associated with a decrease in solute entropy.[39]

3.3. Kinetic−Thermodynamic Corrosion Parameters.

The adsorption process was explained by a thermodynamic model, and the mechanism of corrosion inhibition by the inhibitors was explained by using a kinetic−thermodynamic model. For the corrosion reaction of carbon steel in HCl, the apparent effective activation energies (E_a*) in the presence and absence of inhibitors at various concentrations were calculated from the Arrhenius-type equation (eq 10)[40]

$$(\text{rate})K = A\, e^{-E_a^*/RT} \quad (10)$$

where A is the Arrhenius preexponential factor. A plot of log k (corrosion rate) vs $1/T$ showed straight lines (Figure S6). For the intermediate complex in the transition state for the corrosion of carbon steel in HCl in the absence and presence of inhibitors, the activation entropy (ΔS*) and enthalpy (ΔH*) were calculated using the transition-state equation (eq 11)[41,42]

$$(\text{rate})K = \frac{RT}{Nh} e^{(\Delta S^*/R)} e^{(-\Delta H^*/RT)} \quad (11)$$

where h is Planck's constant and N the Avogadro's number. A plot of log k (corrosion rate)/T vs $1/T$ is a straight line with a slope of $(-\Delta H^*/2.303R)$ and an intercept of $[\log(RT/Nh) + (\Delta S^*/2.303R)]$ as shown in Figure S7.[43,44] The activation energies, enthalpies ΔH*, and entropy ΔS* for the dissolution of the carbon steel in 1.0 M HCl solution with and without inhibitors are collected in Table 4. The inhibitors increased the activation energies of carbon steel, indicating strong adsorption of the molecules of the inhibitors on the metal surface. The entropy of activation ΔS* was negative with and without inhibitors, indicating that the activated complex in the rate-determining step is an association rather than a dissociation step.[45] This implies that the activated molecules were in a higher-order state than the unactivated molecules.[46,47]

3.4. Potentiodynamic Polarization Measurements.

The carbon steel's polarization curves in 1.0 M HCl solution

https://doi.org/10.1021/acsomega.3c02105
ACS Omega 2023, 8, 28314−28332

Table 4. Activation Parameters for the Dissolution of Carbon Steel in the Presence and Absence of Different Concentrations of Inhibitors in 1.0 M HCl

		activation parameters		
inhibitor	conc. × 10^{-5} M	E_a* (kJ mol^{-1})	ΔH* (kJ mol^{-1})	$-\Delta S$* (J mol^{-1} k^{-1})
	1.0 M HCl	22.6	49.5	103.7
CMBTAP	1	25.9	57.3	82.6
	5	26.5	58.5	78.8
	10	26.6	58.6	80.7
	15	27.6	59.8	76.9
	20	27.9	59.9	73.1
CBAN	1	25.3	55.6	86.2
	5	24.2	53.2	94.7
	10	24.8	54.3	92.2
	15	25.6	55.9	85.7
	20	26.4	58.3	82.3
CBAMP	1	24.1	52.9	94.2
	5	25.6	56.1	84.6
	10	26.2	57.7	82.7
	15	26.8	57.9	82.9
	20	27.6	61.2	73.1

with and without CMBTAP, CBAN, and CBAMP at 25 °C are shown in Figure 3a−c, respectively. The anodic and cathodic branches shifted to lower corrosion current densities with the inhibitors, which significantly reduced the rate of corrosion. In other words, the dyes inhibited both cathodic and anodic reactions of carbon steel electrodes in the 1.0 M HCl solution. Table 5 shows the parameters derived from the polarization curves. The addition of dyes did not appreciably alter the Tafel slopes β_a and β_c at 25 °C, showing that the dyes had little impact on the mechanisms of hydrogen evolution and the metal dissolution process. Generally, inhibitors are categorized as cathodic or anodic types if the shift in corrosion potential is more than 85 mV with respect to that in the absence of inhibitors.[48,49] Herein, with the inhibitors, E_{corr} shifted to less negative values, but the shift was very small (20−30 mV), indicating that the dyes are mixed-type inhibitors with predominant anodic characteristics.[50] IE% increased with increasing concentration of the dyes as shown in Figure 3d, and the inhibition efficiency of the dyes evaluated using the polarization method declined in the following order: CMBTAP > CBAMP > CBAN. This sequence matches that obtained by measurements of weight loss.

3.5. Electrochemical Impedance Spectroscopy. Nyquist and Bode diagrams of carbon steel in 1.0 M HCl solutions containing various concentrations of CMBTAP, CBAN, and CBAMP at 25 °C are shown in Figures 4a−c and S8, respectively. A single depressed semicircle can be seen in each impedance spectrum. With an increase in dye concentration, the semicircle's diameter increased. The single capacitive loop

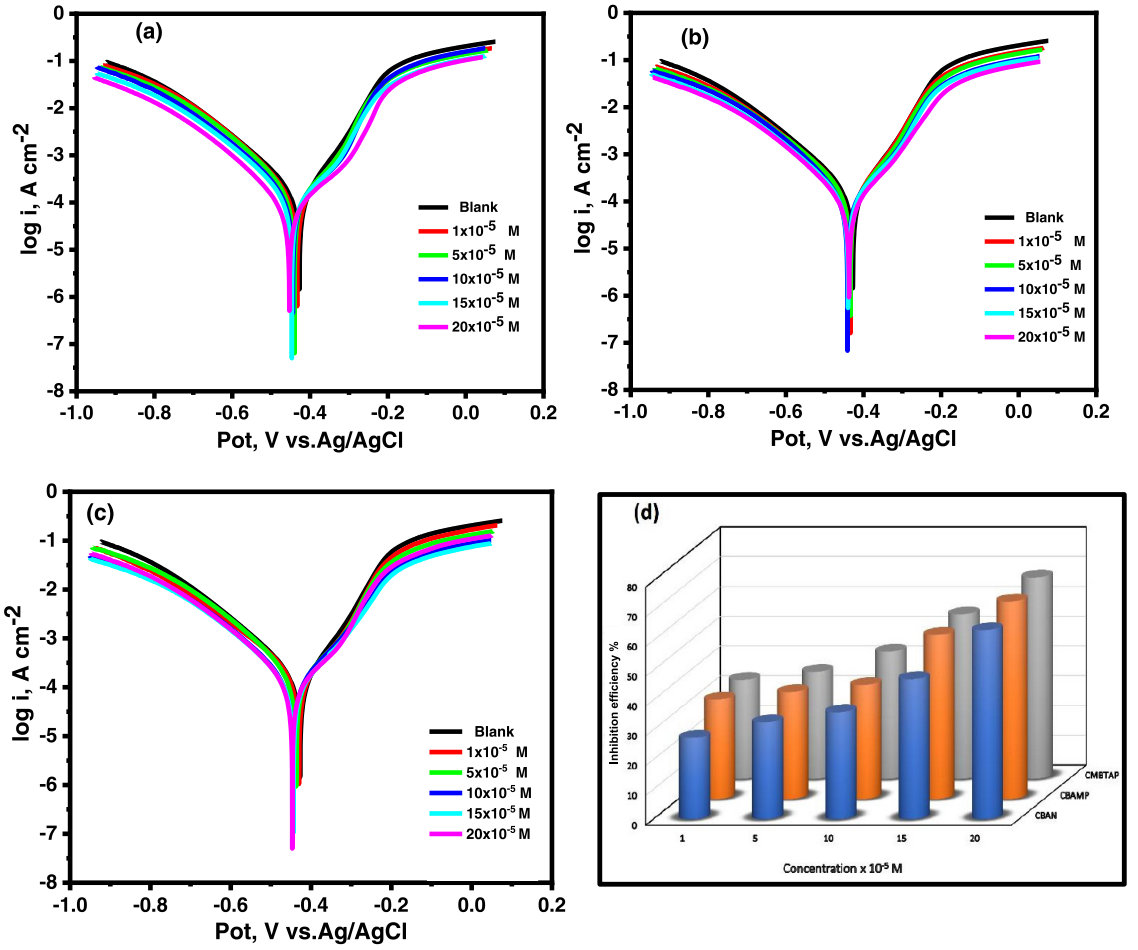

Figure 3. Potentiodynamic polarization curves for the corrosion of carbon steel in 1.0 M HCl of the inhibitors (a) CMBTAP, (b) CBAN, (c) CBAMP, and (d) inhibition efficiency (IE%) at different concentrations (1 × 10^{-5} to 20 × 10^{-5} M) at 25 °C.

https://doi.org/10.1021/acsomega.3c02105
ACS Omega 2023, 8, 28314−28332

Table 5. Effect of Concentration of the Investigated Compounds on the Free Corrosion Potential (E_{corr}), Corrosion Current Density (i_{corr}), Tafel Slopes (β_a and β_c), Corrosion Rate (C.R.), Degree of Surface Coverage θ, and Inhibition Efficiency (%IE) for the Corrosion of Carbon Steel in 1.0 M HCl at 25 °C

inhibitor	conc. × 10^{-5} (M)	$-E_{corr}$ (Mv)	i_{corr} (μA cm^2)	β_c (mV dec^{-1})	β_a (mV dec^{-1})	corrosion rate (CR) (mp y^{-1})	θ	%IE
CMBTAP	blank	420	118.5	125.77	86.8	55.36		
	1	425	78.94	116.9	100.16	40.7	0.333	33.3
	5	441	75.8	79.12	100.04	35.4	0.36	36
	10	445	67.9	78.96	96.9	31.72	0.427	42.7
	15	449	52.9	71.89	89.7	24.7	0.553	55.3
	20	453	38.18	78.24	93.8	17.8	0.677	67.7
CBAN	1	423	86.12	126.1	89.4	42.4	0.273	27.3
	5	430	80.1	99.74	87.7	37.65	0.325	32.5
	10	439	75.8	99.1	102.9	35.4	0.36	36
	15	440	62.8	86.1	98.9	29.3	0.471	47.1
	20	431	43.15	74.07	69.48	20.08	0.605	63.5
CBAMP	1	425	78.9	95.8	90.2	36.8	0.334	33.4
	5	430	76.67	87.6	100.3	35.3	0.359	35.9
	10	438	73.03	101.9	95.25	33.5	0.383	38.3
	15	443	53.2	80.1	82.4	25.5	0.551	55.1
	20	447	42.8	60.5	70.66	19.9	0.64	66.4

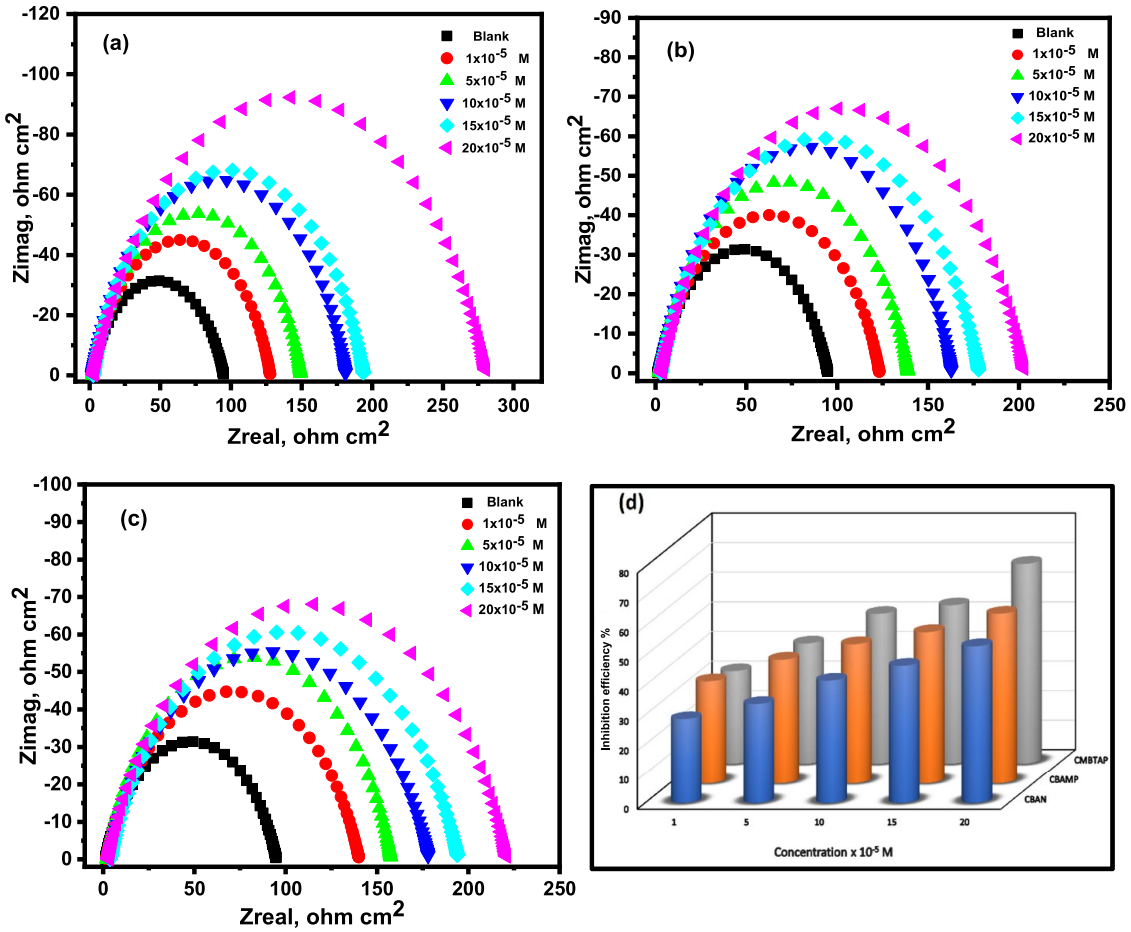

Figure 4. Nyquist plots for corrosion of carbon steel in 1.0 M HCl of the inhibitors (a) CMBTAP, (b) CBAN, (c) CBAMP, and (d) inhibition efficiency (IE%) at different concentrations (1 × 10^{-5} to 20 × 10^{-5} M) at 25 °C.

exhibited in the impedance spectra indicates that charge transfer primarily regulates carbon steel corrosion,[51] and the dyes have no effect on the dissolution mechanism of carbon steel.[52] In comparison to the blank solution, the capacitive loop's diameter grew wider with increasing inhibitor concentration. This demonstrates that the impedance of the inhibited substrate increases with the inhibitor concentration.[53] This behavior is related to the inhomogeneous metal surface caused by interfacial phenomena or surface roughness,[54] which are frequent in solid metal electrodes.[55] Generally, when a nonideal frequency response is obtained, distributed circuit elements can be employed in the equivalent circuits. The constant phase element

https://doi.org/10.1021/acsomega.3c02105
ACS Omega 2023, 8, 28314−28332

(CPE) is the most widely used and has a noninteger power dependence on the frequency.[56] Therefore, in this study, the equivalent circuit shown in Figure S9 was used to investigate the impedance spectra, where R_s represents the solution resistance, R_{ct} the charge-transfer resistance, and CPE the interfacial capacitance. The values of R_s and R_{ct} obtained from EIS fitting and IE% are listed in Table 6. R_{ct} increased with an increase in the concentration of the dyes, indicating a decrease in the corrosion rate and increase in the inhibition efficiencyFigure 4d. The sequence of IE% from EIS measurements is CMBTAP > CBAMP > CBAN, which is congruent with the IE% obtained from weight-loss and polarization measurements.

Table 6. Electrochemical Kinetic Parameters Obtained by the EIS Technique in 1.0 M HCl without and with Various Concentrations of Investigated Compounds at 25 °C

inhibitor	conc. × 10^{-5} M	R_{ct} (Ω cm^2)	θ	%IE
CMBTAP	1.0 M HCl	93.5		
	1	136	0.312	31.25
	5	157.4	0.406	40.6
	10	189.5	0.506	50.6
	15	201.3	0.535	53.5
	20	288.2	0.675	67.5
CBAN	1.0 M HCl	93.5		
	1	129.2	0.286	28.6
	5	140.9	0.337	33.7
	10	160.23	0.416	41.6
	15	175.3	0.466	46.6
	20	200.1	0.532	53.2
CBAMP	1.0 M HCl	93.5		
	1	143.09	0.346	34.6
	5	160.96	0.419	41.9
	10	176.87	0.4713	47.13
	15	191.59	0.512	51.2
	20	220.3	0.575	57.4

3.6. Synergistic Inhibition Effect of Iodide Ions. As aforementioned, the addition of halide ions, such as I^-, Br^-, and Cl^-, to corrosive media increases the adsorptivity of organic cations by forming interconnecting bridges between the negatively charged metal surface and the inhibitor cations. I^- has the strongest synergistic effect than other halides owing to its large ionic radius, high hydrophobicity, and high polarizability. Thus, herein, KI was used to increase the IE of the synthesized dyes.

Figure 5a−c shows the potentiodynamic polarization curves for carbon steel in 1.0 M HCl with various doses of the dyes in 0.01 M KI. The diagrams show that the addition of dyes alone to the acid environment shifted the cathodic corrosion current, whereas the addition of dyes and KI changed E_{corr} to a more cathodic value compared with that of the blank solution. The changes in the E_{corr} of HCl and CBAMP, CBAN, and CMBTAP systems were −27, −20, and −30 mV/Ag/AgCl, respectively (Table 5), whereas those of CBAMP, CBAN, and CMBTAP with KI were −50, −45, and −56 mV/Ag/AgCl, respectively. Table 7 demonstrates that i_{corr} was substantially decreased when 0.01 M KI was added to the dye solutions, and IE% increased from 66.4 to 90.5, 63.5 to 84.2, and 67.7 to 93.2 for CBAMP, CBAN, and CMBTAP, respectively. The combination of the dyes and 0.01 M KI showed better IE% than the case of only the dyes for all inhibitor concentrations as shown in Figure 5d.The high corrosion inhibition efficiencies of the solutions containing KI are attributed to the strong chemisorption of iodide ions on metal surfaces.[57] Thus, azo dye molecules are adsorbed on the metal surface by Coulombic attractions. The stabilization of the adsorbed iodide ions with the dyes results in more surface coverage and, therefore, more inhibition effects.[58] The iodide ions improved the stability of the dyes on the metal surface through a coadsorption mechanism, which may be either competitive or cooperative.[59] For competitive adsorption, the anions and inhibitor cations are adsorbed on the metal surface at distinct locations. In cooperative adsorption, the anions are chemisorbed on the metal surface, and the cations are adsorbed on a layer of the anions. In some cases, both competitive and cooperative mechanisms occur.[60]

The effect of KI on the IE% of the synthesized dyes was observed by EIS. Figure 6 shows the Nyquist impedance diagrams for the carbon steel in a corrosive environment with different concentrations of dyes and 0.01 M KI. As seen in the capacitive loop of the diagrams in comparison to those of CMBTAP, CBAN, and CBAMP alone, adding KI to the solution improved the dyes' protection capabilities. The corrosion rate decreased markedly with the addition of 0.01 M KI (Table 8). Beyond this concentration, the corrosion rate decreased gradually, attributed to the increase in the surface coverage (θ) of the dye molecules on metal surfaces with increasing concentration. The corrosion IE% also increased with increasing concentrations of CBAMP, CBAN, and CMBTAP. With a dye concentration of 2×10^{-4} M, maxima IE% (60.3, 58.4, and 70.7, respectively) were obtained (Table 6), indicating that a single dye cannot effectively protect carbon steel from corrosion in HCl. Table 8 also lists IE% for a constant KI concentration (0.01 M) and varying concentrations of dyes in a 1.0 M HCl solution. Compared with the inhibition efficiency values of the inhibitor (without KI), the combination of the dyes and 0.01 M KI showed better IE% than the case of only the dyes for all inhibitor concentrations as shown in Figure 6d.

The interaction between KI and the dye molecules can be described by introducing a synergism parameter S_θ, which was proposed by Aramaki and Hackerman[61] and is expressed as follows

$$S_\theta = \frac{1 - \theta_{1+2}}{1 - \theta'_{1+2}} \tag{12}$$

where $\theta_{1+2} = (\theta_1 + \theta_2) - (\theta_1\theta_2)$; θ_1 and θ_2 are the surface coverage by KI and the dye, respectively, and θ'_{1+2} is the measured surface coverage by the dyes combined with KI. S_θ is close to 1 when there is no interaction between the dye molecules and the iodide ions, greater than 1 when there is a synergistic effect, and less than 1 when there is an antagonistic interaction resulting from competitive adsorption. The values of S_θ for different inhibitor concentrations combined with KI are listed in Table S1. All S_θ values are greater than unity, indicating strong inhibition effects on carbon steel owing to the synergistic effect of I^-, which is initially adsorbed on the metal surface, followed by inhibitor cations. Moreover, the adsorption of both I^- and dye cations decreases the positive charge of Fe due to the formation of Fe−I^- bonds, which suppress the rate of autocorrosion.

3.7. Surface Examination. *3.7.1. Scanning Electron Microscopy.* The morphology of a polished carbon steel electrode before being exposed to a blank corrosive medium is shown in Figure 7a. The specimens were examined by SEM at ×500 magnification. The micrograph shows characteristic

https://doi.org/10.1021/acsomega.3c02105
ACS Omega 2023, 8, 28314−28332

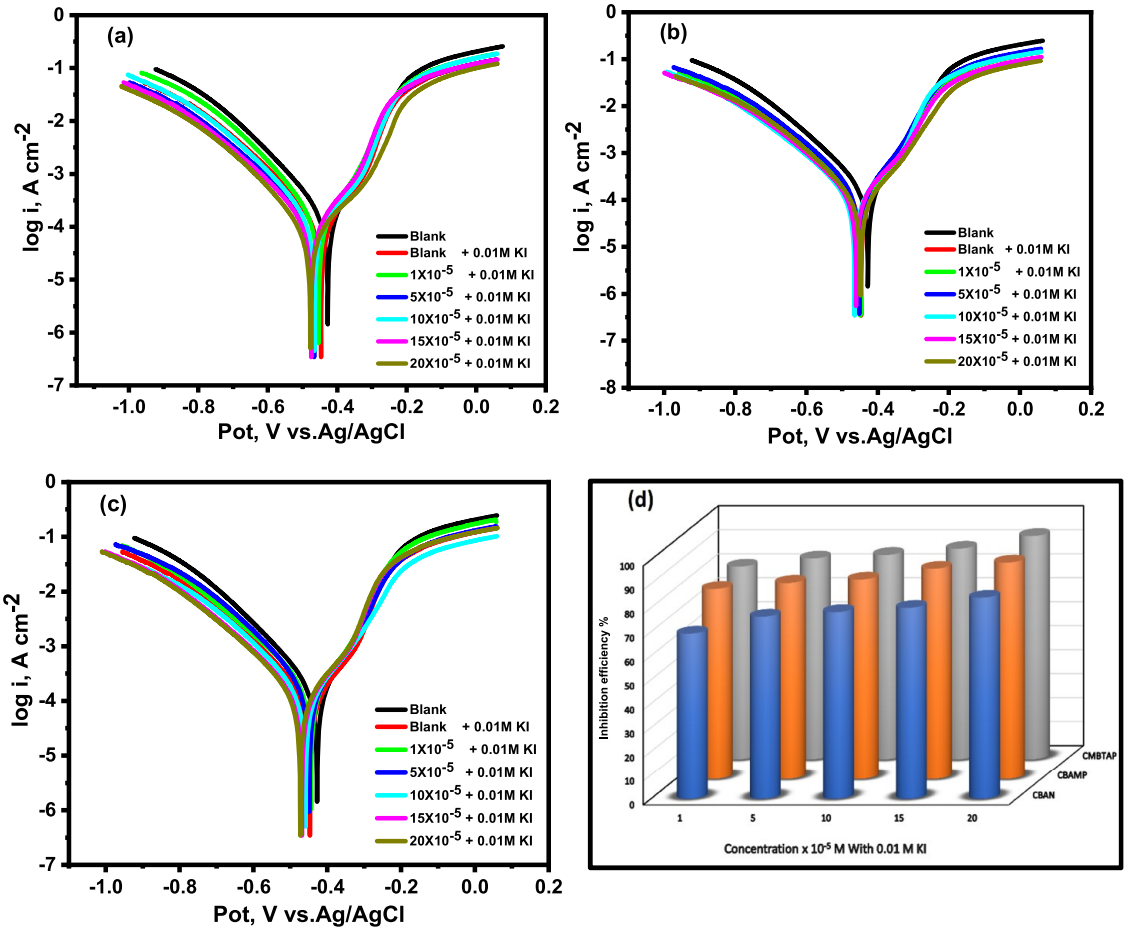

Figure 5. Potentiodynamic polarization curves for the corrosion of carbon steel in 1.0 M HCl of the inhibitors (a) CMBTAP, (b) CBAN, (c) CBAMP, and (d) inhibition efficiency (IE%) at different concentrations (1×10^{-5} to 20×10^{-5} M) in the presence of KI at 25 °C.

Table 7. Potentiodynamic Polarization Data for Carbon Steel in 1.0 M HCl with and without KI and Inhibitors + KI at 25 °C

inhibitors	conc. (M)	$-E_{corr}$ (Mv)	i_{corr} (μA cm^2)	β_c (mV dec^{-1})	β_a (mV dec^{-1})	corrosion rate (CR) (mp y^{-1})	θ	%IE
CMBTAP	blank (1.0 M HCl)	420	118.5	125.77	86.8	55.36		
	0.01 M KI	443.7	66.4	101.85	93.66	30.59	0.428	22.8
	1×10^{-5} + 0.01 M KI	448	23.2	95.04	107.7	10.93	0.804	80.4
	5×10^{-5} + 0.01 M KI	464	19.09	64.32	107.5	8.5	0.838	83.8
	10×10^{-5} + 0.01 M KI	446	17.42	64.2	104.2	7.75	0.853	85.3
	15×10^{-5} + 0.01 M KI	472	14.23	58.5	96.4	5.25	0.879	87.9
	20×10^{-5} + 0.01 M KI	476	8.1	63.6	100.8	3.75	0.932	93.2
CBAN	1×10^{-5} + 0.01 M KI	446	36.5	102.5	96.2	18.9	0.692	69.2
	5×10^{-5} + 0.01 M KI	453	28.1	81.1	94.3	14.1	0.763	76.3
	10×10^{-5} + 0.01 M KI	462	25.9	80.5	110.6	12.1	0.782	78.2
	15×10^{-5} + 0.01 M KI	465	23.5	70.0	106.3	11.2	0.80	80
	20×10^{-5} + 0.01 M KI	451	18.8	60.3	74.7	8.74	0.842	84.2
CBAMP	1×10^{-5} + 0.01 M KI	445	24.4	77.9	96.9	11.3	0.795	79.5
	5×10^{-5} + 0.01 M KI	453	21.6	71.5	107.8	10.1	0.82	82
	10×10^{-5} + 0.01 M KI	461	19.7	83.0	102.4	8.95	0.834	83.4
	15×10^{-5} + 0.01 M KI	466	14.3	65.1	88.6	6.8	0.879	87.9
	20×10^{-5} + 0.01 M KI	470	11.5	50.5	76.0	5.3	0.905	90.5

inclusion, which could be an oxide inclusion. Figure 7b shows the SEM image of the surface of the carbon steel electrode specimen after 24 h immersion in a 1.0 M HCl solution. The electrode's surface has significant damage. The specimen's corroded regions are shown as black grooves with gray and white zones that resemble the dandruff of iron oxide. This indicates that the uncovered surface of the metal electrode was severally corroded. We infer that the highly oxidized phase was formed in air when desiccated without protection on the surface. Figure 7c–e shows SEM images of the surface of a carbon steel specimen after 24 h immersion in a 1.0 M HCl solution with higher concentrations (20×10^{-5} M) of CMBTAP, CBAN, and CBAMP. The metal surface was smoother than that of the specimen immersed in the acid solution without the dyes. A

https://doi.org/10.1021/acsomega.3c02105
ACS Omega 2023, 8, 28314−28332

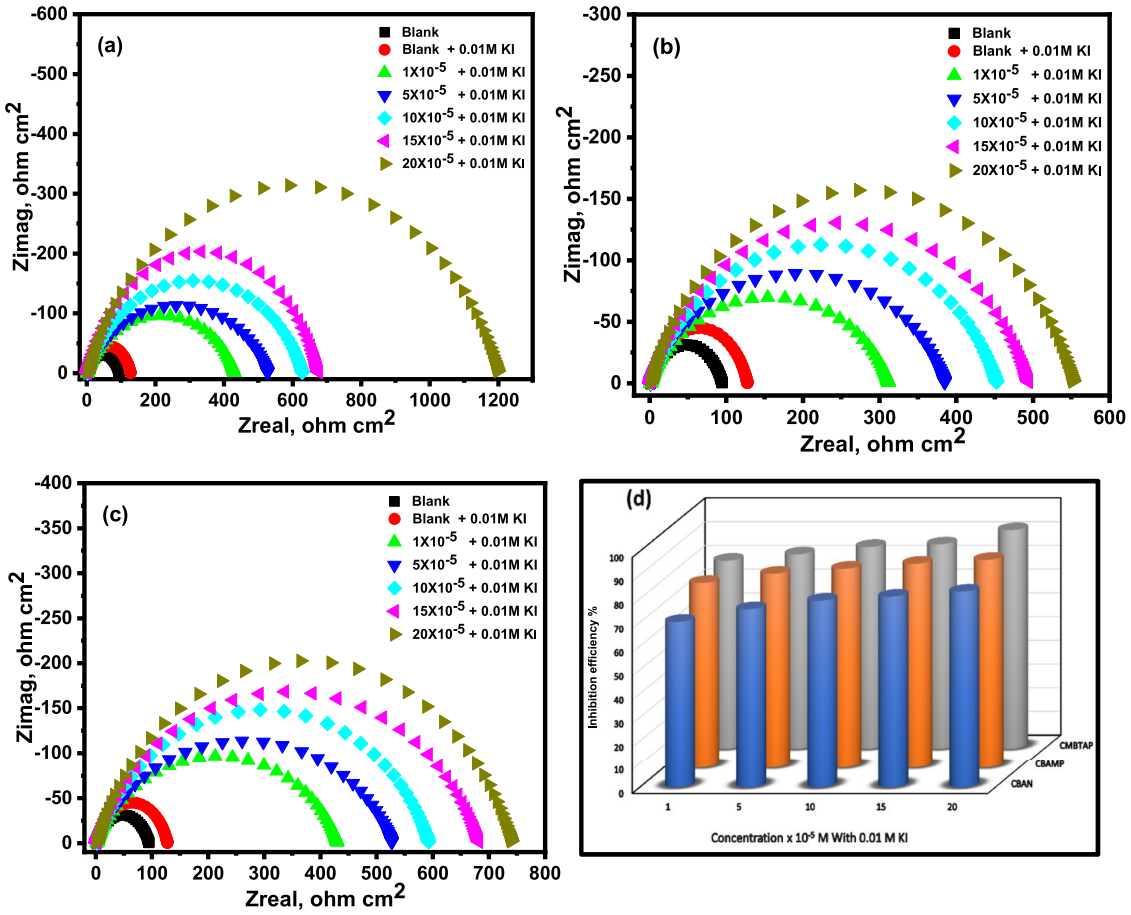

Figure 6. Nyquist diagrams for carbon steel in 1.0 M HCl of the inhibitors (a) CMBTAP, (b) CBAN, (c) CBAMP, and (d) inhibition efficiency (IE%) at different concentrations (1×10^{-5} to 20×10^{-5} M) in the presence of KI at 25 °C.

Table 8. Impedance Parameters for Carbon Steel in 1.0 M HCl with and without KI and Inhibitors + KI

inhibitor	conc. (M)	R_{ct} (Ω cm^2)	θ	%IE
CMBTAP	blank (1.0 M HCl)	93.5		
	0.01 M KI	120.5	0.224	22.4
	1×10^{-5} + 0.01 M KI	452.2	0.793	79.3
	5×10^{-5} + 0.01 M KI	522.5	0.82	82
	10×10^{-5} + 0.01 M KI	628.9	0.851	85.1
	15×10^{-5} + 0.01 M KI	675.8	0.862	86.2
	20×10^{-5} + 0.01 M KI	1200.2	0.922	92.2
CBAN	1×10^{-5} + 0.01 M KI	314.3	0.703	70.3
	5×10^{-5} + 0.01 M KI	383.2	0.756	75.6
	10×10^{-5} + 0.01 M KI	448.8	0.792	79.2
	15×10^{-5} + 0.01 M KI	490.9	0.809	80.9
	20×10^{-5} + 0.01 M KI	550.5	0.83	83
CBAMP	1×10^{-5} + 0.01 M KI	430.1	0.783	78.3
	5×10^{-5} + 0.01 M KI	525.5	0.822	82.2
	10×10^{-5} + 0.01 M KI	597.0	0.843	84.3
	15×10^{-5} + 0.01 M KI	686.3	0.864	86.4
	20×10^{-5} + 0.01 M KI	780.5	0.8802	88.02

good protective film was formed on the metal surface. This corroborates the high IE% of the dyes. Figure 7f–h shows SEM images of the surface of a carbon steel specimen after 24 h immersion in a 1.0 M HCl solution containing 20×10^{-5} M dyes and 0.01 M KI. The metal surface was the smoothest, indicating better inhibition, which is attributed to the synergistic effect of the dyes and iodide ions.

3.7.2. Energy Dispersive X-ray Spectroscopy. Figure 8 a,b shows the EDX spectra of the surface of the carbon steel sample in the absence and presence of 1.0 M HCl. Figure 8c–e shows the EDX spectra of the surface of the carbon steel sample immersed in a 1.0 M HCl solution containing 20×10^{-5} M CMBTAP, CBAN, and CBAMP, and Figure 8f–h shows those of the sample immersed in a 1.0 M HCl solution containing 20×10^{-5} M dyes and 0.01 M KI. Table 9 lists the various elements' atomic percentages on the polished, uninhibited, and inhibited carbon steel surfaces as determined by EDX. The atomic percentage of iron in the carbon steel sample immersed in a 1.0 M HCl solution is 81.94%, those of the samples immersed in the solution containing 20×10^{-5} M CMBTAP, CBAN, and CBAMP are 78.84, 79.28, and 81.51%, respectively, and those of the samples immersed in a solution containing 20×10^{-5} M CMBTAP, CBAN, and CBAMP and 0.01 M KI are 81.30, 68.81, and 78.01%, respectively. The spectra of the samples immersed in the solution containing the dyes and 0.01 M KI show smooth iron peaks compared to those of the samples polished and immersed in the solution with the dyes. This suppression of iron lines indicates the formation of a more corrosion-inhibiting film on the sample surface. EDX spectra of the inhibited samples show peaks corresponding to all constituent elements of the dye molecules, indicating the adsorption of the dye molecules on the surface of the samples.

3.7.3. Atomic Force Microscopy (AFM). AFM is a powerful tool for investigating the morphology of the carbon steel surface in the absence and presence of the optimum concentrations of

https://doi.org/10.1021/acsomega.3c02105
ACS Omega 2023, 8, 28314−28332

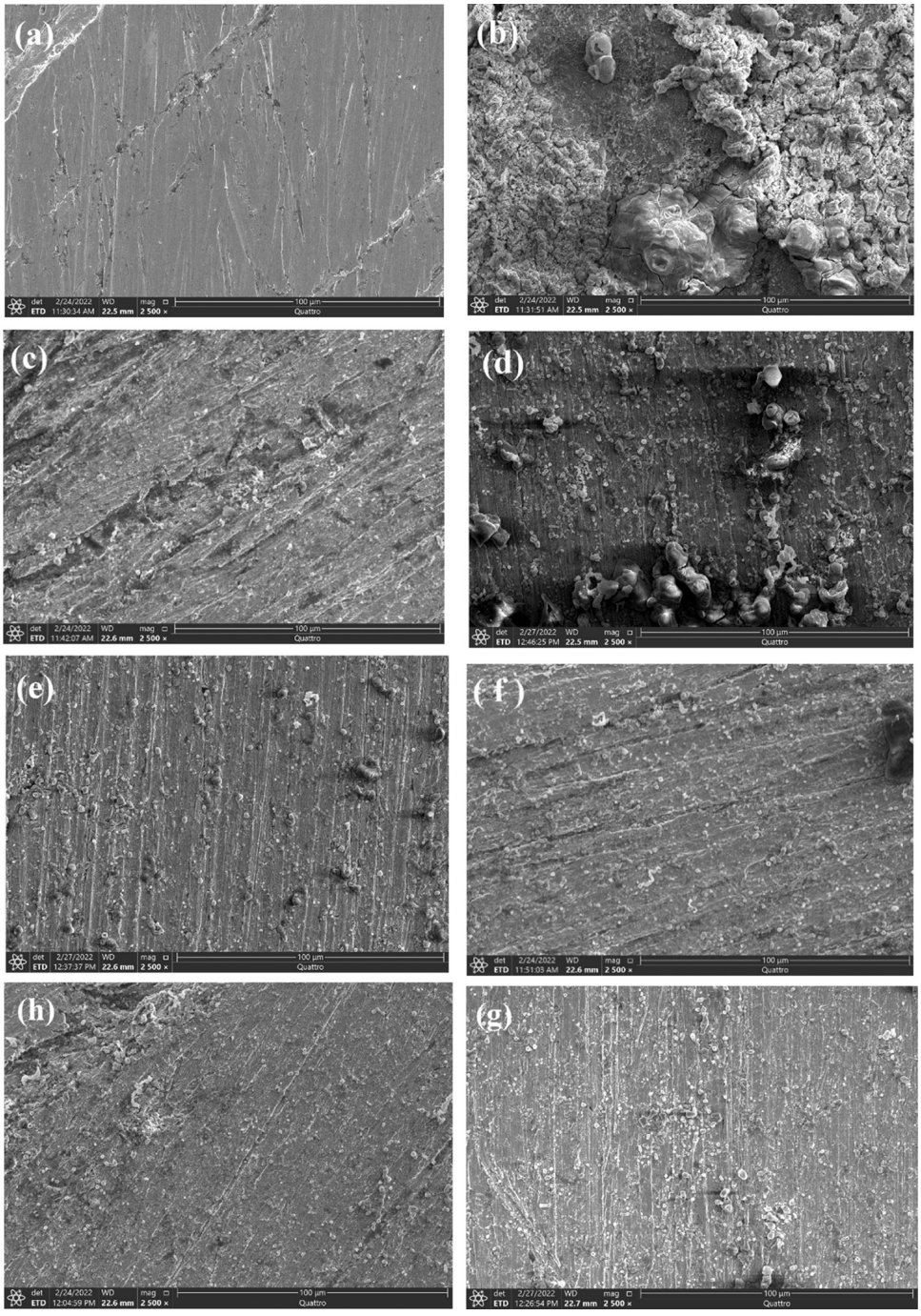

Figure 7. SEM micrographs of the carbon steel surface (a) before immersion in 1.0 M HCl, (b) after 24 h of immersion in 1.0 M HCl, (c−e) after 24 h of immersion in 1.0 M HCl + 20×10^{-5} M benzothiazole dyes CMBTAP, CBAN, and CBAMP, respectively, and (f−h) after 24 h of immersion in 1.0 M HCl + 20×10^{-5} M benzothiazole dyes CMBTAP, CBAN, and CBAMP in the presence of 0.01 M KI, respectively, at 25 °C.

inhibitors, which are combined with SEM and provide additional evidence of the adsorption of inhibitor molecules on the surface of the metal. The surface roughness values, namely, the quadratic roughness (R_q), mean roughness (R_a), and maximum roughness (R_{max}), are summarized in Table 10. Figure 9 showed three-dimensional (3D) AFM images of the carbon steel surface before exposure to corrosive media, after 24 h immersion in a 1.0 M HCl solution, after 24 h immersion in a 1.0 M HCl solution with higher concentrations (20×10^{-5} M) of CMBTAP, CBAN, and CBAMP, and after 24 h immersion in a 1.0 M HCl solution containing 20×10^{-5} M dyes and 0.01 M KI. As can be seen, the carbon steel surface after 24 h immersion in a 1.0 M HCl solution was strongly corroded and destroyed compared to the smooth surface of pure carbon steel, and the surface roughness values (R_q, R_a, and R_{max}) were higher than the pure carbon steel Figure 9b. The metal surface after 24 h immersion in a 1.0 M HCl solution with higher concentrations (20×10^{-5} M) of CMBTAP and CBAN was less destroyed and became smoother than that of the specimen immersed in the acid solution without the dyes, and the surface roughness values were lower than the carbon steel in acidic solution Figure 9c−e. However, the carbon steel surface after 24 h immersion in a 1.0

https://doi.org/10.1021/acsomega.3c02105
ACS Omega 2023, 8, 28314−28332

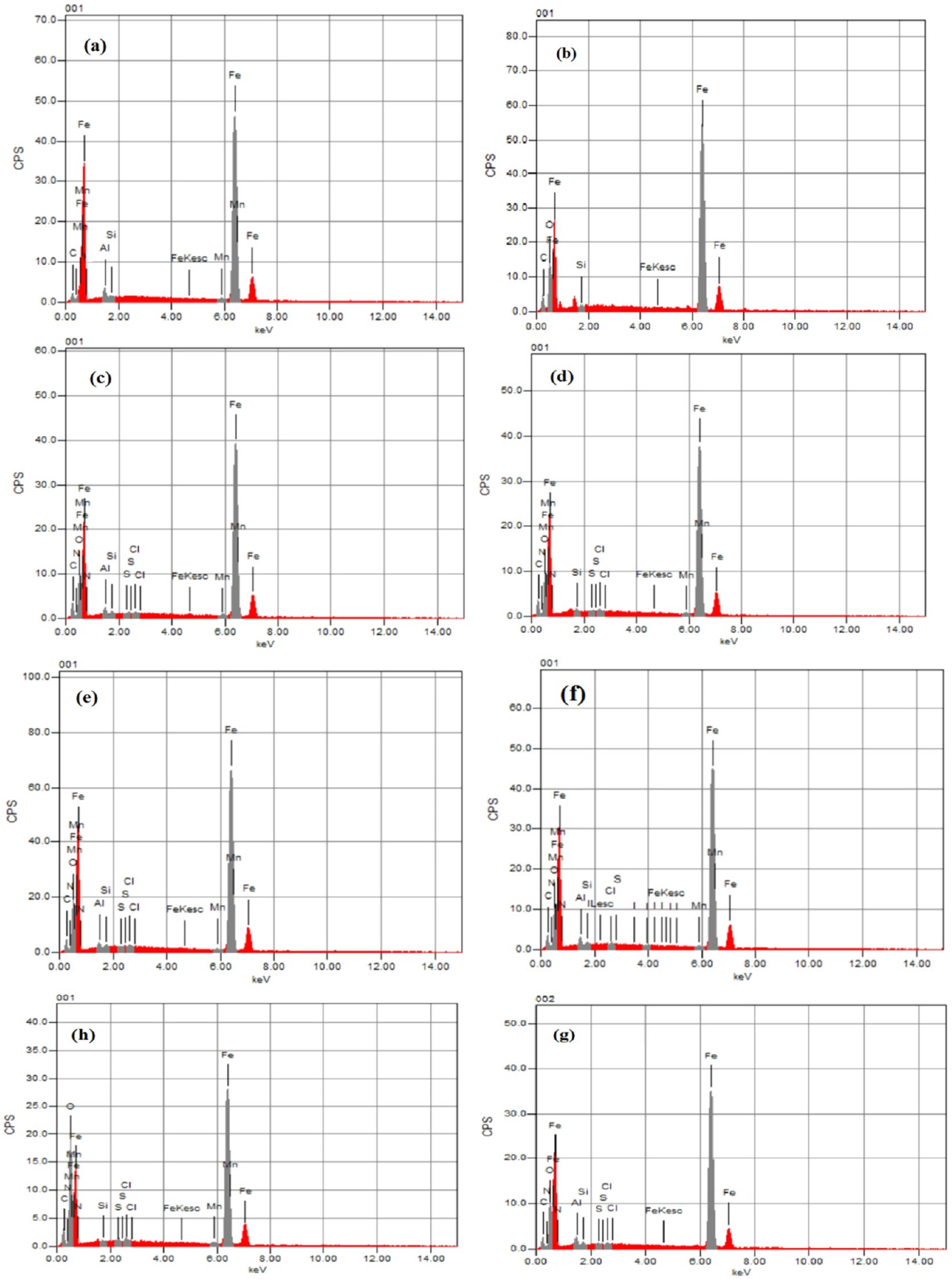

Figure 8. EDX analysis of the carbon steel surface (a) before immersion in 1.0 M HCl, (b) after 24 h of immersion in 1.0 M HCl, (c−e) after 24 h of immersion in 1.0 M HCl + 20×10^{-5} M benzothiazole dyes CMBTAP, CBAN, and CBAMP, respectively, and (f−h) after 24 h of immersion in 1.0 M HCl + 20×10^{-5} M benzothiazole dyes CMBTAP, CBAN, and CBAMP in the presence of 0.01 M KI, respectively, at 25 °C.

https://doi.org/10.1021/acsomega.3c02105
ACS Omega 2023, 8, 28314−28332

Table 9. Percentage Atomic Contents of Elements Obtained from EDX Spectra

inhibitors	Fe	Mn	Al	Si	Cl	C	O	N	S	I
carbon steel (free)	91.29	0.88	2.13	0.78		4.92				
carbon steel in 1.0 M HCl	81.94			0.17		8.06	9.83			
CMBTAP	78.84	0.73	1.16	0.29	0.34	8.72	8.96	0.87	0.09	
CBAN	79.28	0.83		0.44	0.25	8.80	8.74	1.64	0.03	
CBAMP	81.51	0.64	0.67	0.35	0.19	6.19	9.64	0.80	0.02	
CMBTAP + 0.01 M KI	81.30	0.79	1.02	0.23	0.14	7.15	7.71	1.46	0.04	0.19
CBAN + 0.01 M KI	68.81	0.83		0.19	0.33	6.68	22.5	0.56	0.09	
CBAMP + 0.01 M KI	78.07		1.24	0.36	0.36	7.49	10.99	1.42	0.07	

Table 10. Roughness Values Obtained from AFM for the Carbon Steel Surface in 1.0 M HCl with and without Inhibitors and Inhibitors + KI

inhibitors	R_a (nm)	R_q (nm)	R_{max} (nm)
carbon steel (free)	191.5	271.7	4098
carbon steel in 1.0 M HCl	840	1038	6980
CMBTAP	509.2	688.4	4698.2
CBAN	615	808.7	5029.4
CBAMP	585.6	758.2	5076.4
CMBTAP + 0.01 M KI	313.3	481.6	4680
CBAN + 0.01 M KI	468.5	621.8	4706
CBAMP + 0.01 M KI	358.5	529.9	4506

M HCl solution containing 20×10^{-5} M dyes and 0.01 M KI was the smoothest and the surface roughness values were lowest, indicating better inhibition that attributed to the synergistic effect of the dyes and iodide ions Figure 9f–h.

3.8. Quantum Chemical Calculations. Based on the above experimental results, the inhibition efficiencies of the dyes are in the order CMBTAP > CBAMP > CBAN. The high IE% of CMBTAP is attributed to the high number of adsorption sites on its molecules.[62]

Moreover, quantum chemical simulations were used to examine the effect of structural parameters on the IE% and the adsorption mechanisms of the dyes on the metal surface. The bond lengths, bond angles, and dihedral angles of the dyes were optimized to obtain their geometric and electrical structures. Figure S10 shows the optimized molecular structures with the lowest energies.

The obtained quantum chemical parameters are listed in Table 11 and include the energies of the highest occupied and lowest unoccupied molecular orbitals (E_{HOMO} and E_{LUMO}), the separation energy ΔE (=$E_{LUMO} - E_{HOMO}$), which is a function of reactivity, the dipole moment (D), electronegativity (χ), chemical potential (μ), softness (σ), and hardness (η). According to Koopman's theorem, the dyes' E_{HOMO} and E_{LUMO} are connected to the ionization potential (I) and electron affinity (A), respectively.[63] Other quantum chemical parameters that provide useful information about the reactivity of the dyes are calculated as follows[64,65]

$$\chi\ (\text{electronegativity}) = \frac{-(E_{LUMO} + E_{HOMO})}{2} \quad (13)$$

$$\mu\ (\text{potential}) = -\chi = \frac{(E_{LUMO} + E_{HOMO})}{2} \quad (14)$$

$$\eta\ (\text{hardness}) = \frac{(E_{LUMO} - E_{HOMO})}{2} \quad (15)$$

$$\omega\ (\text{electrophilicity}) = \mu^2/2\eta \quad (16)$$

Softness is defined as the inverse of global hardness, expressed as follows

$$\sum (\text{softness}) = 1/\eta \quad (17)$$

The fraction of electrons (ΔN) transferred between the inhibitors and the metallic surface is expressed as follows[66]

$$\Delta N = \frac{(\chi_{Fe} - \chi_{inh})}{2(\eta_{Fe} + \eta_{inh})} \quad (18)$$

where a theoretical value of $\chi_{Fe} \approx 7$ eV and $\eta_{Fe} = 0$, assuming that $I = A$ for bulk metals because they are softer than neutral metallic atoms.

The frontier molecular orbital theory states that the interaction between the highest occupied molecular orbital (HOMO) and lowest unoccupied molecular orbital (LUMO) of the interacting species determines chemical reactivity.[67] Although E_{LUMO} indicates a molecule's ability to accept electrons, E_{HOMO} indicates its ability to donate electrons to an acceptor with empty molecular orbitals. The lower the E_{LUMO}, the higher the ability of the molecule to accept electrons.[68] The high E_{HOMO} of the dyes demonstrates how easily they may provide electrons to the unoccupied d-orbital of the metal surface, leading to a high corrosion efficiency (IE%).

CMBTAP showed the highest E_{HOMO} (−5.083 eV, Table 11), indicating its high tendency to adsorb on metal surfaces and, thus, its high IE%, which is consistent with the experimental results. Energy gap, $\Delta E_{gap} = E_{HOMO} - E_{LUMO}$, is a significant stability index for developing theoretical models to explain the structure and conformational barriers in many molecular systems. The lower the value of ΔE, higher the corrosion IE% of the molecule.[69,70] The calculations revealed that CMBTAP has the smallest energy gap (2.041 eV) among the synthesized dyes. Thus, CMBTAP would have a higher tendency to adsorb on metal surfaces than the other dyes.

Absolute hardness η and softness σ are crucial variables to measure a molecule's stability and reactivity. Soft molecules have low energy gaps compared to hard molecules' high energy gaps. Soft molecules are more reactive than hard ones as they may supply electrons to an acceptor more readily. Adsorption occurs at the part of the molecule where σ, which is a local property, has the highest value.[68] The inhibitor acts as a Lewis base and the metal as a Lewis acid in a corrosive system. Soft base inhibitors are most effective against the acidic corrosion of metals because bulk metals are soft acids. Thus, CMBTAP, which has the highest σ value (0.9799 eV^{-1}), would have the highest IE%, which agrees well with the experimental data. Furthermore, the calculations revealed that CMBTAP has the lowest χ (4.06 eV), which increases its ability to donate electrons to metal surfaces and, therefore, improves its IE.

https://doi.org/10.1021/acsomega.3c02105
ACS Omega 2023, 8, 28314−28332

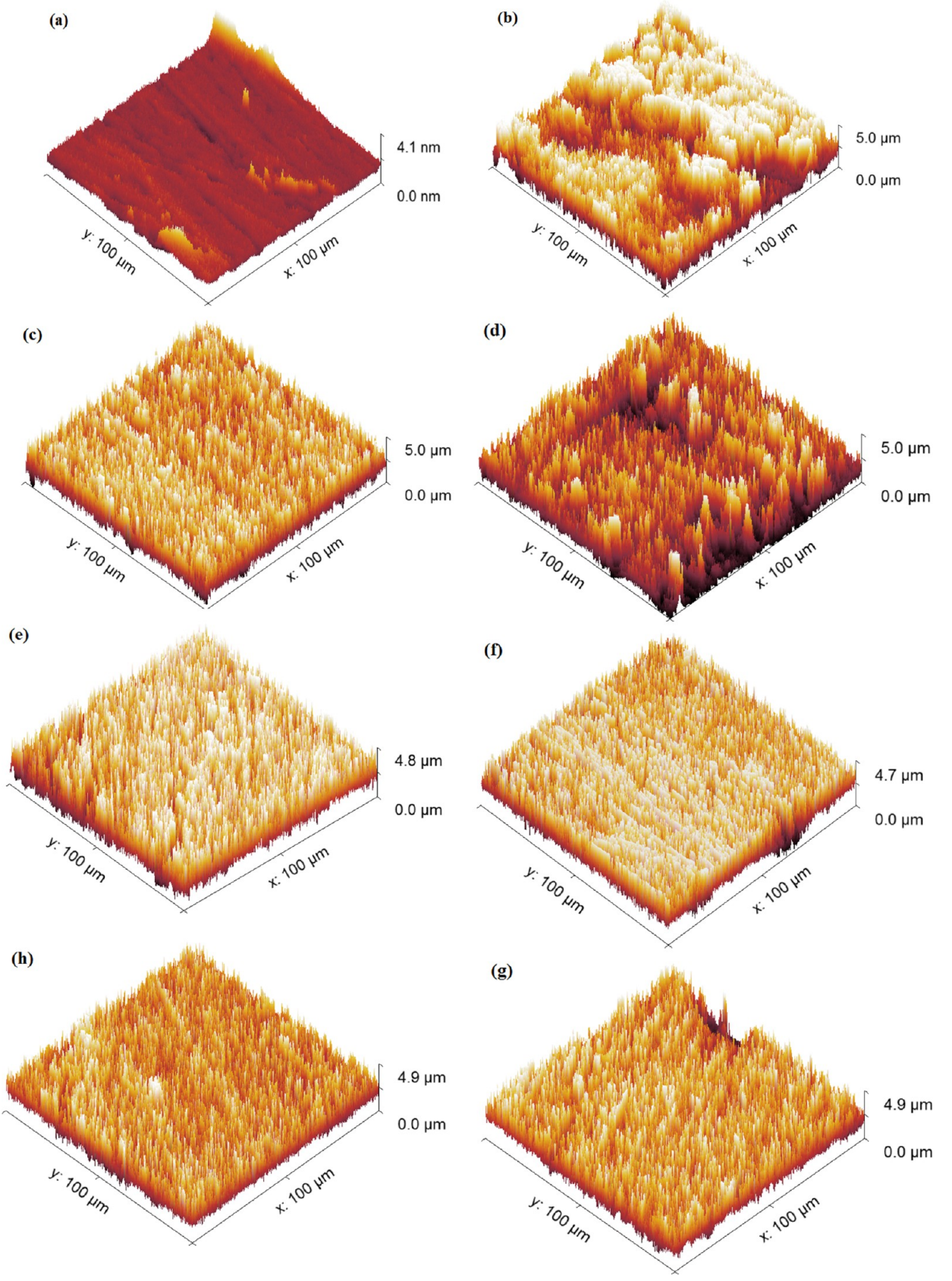

Figure 9. AFM images of the carbon steel surface (a) before immersion in 1.0 M HCl, (b) after 24 h of immersion in 1.0 M HCl, (c–e) after 24 h of immersion in 1.0 M HCl + 20×10^{-5} M benzothiazole dyes CMBTAP, CBAN, and CBAMP, respectively, and (f–h) after 24 h of immersion in 1.0 M HCl + 20×10^{-5} M benzothiazole dyes CMBTAP, CBAN, and CBAMP in the presence of 0.01 M KI, respectively, at 25 °C.

https://doi.org/10.1021/acsomega.3c02105
ACS Omega 2023, 8, 28314−28332

Table 11. Calculated Quantum Chemical Parameters Obtained from Dmol^3 Calculations

inhibitor name	E_{HOMO} (eV)	E_{LUMO} (eV)	ΔE (eV)	D (Debye)	η (eV)	σ (eV^{-1})	μ (eV)	χ (eV)	ω (eV)	ΔN
CMBTAP	−5.083	−3.042	2.041	3.1113	1.021	0.9799	−4.06	4.06	8.08619	1.44
CBAN	−5.776	−3.368	2.408	0.9636	1.204	0.8305	−4.57	4.57	8.68072	1.01
CBAMP	−5.367	−2.973	2.394	3.4528	1.197	0.8354	−4.17	4.17	7.26353	1.18

ΔN measures the ease of electron transfer from an inhibitor to the metal if $\Delta N > 0$ and vice versa. Lukovits et al.[71] reported that when $\Delta N < 3.6$, the ability of the molecules to donate electrons to metal surfaces increases. The ΔN of CMBTAP is somewhat greater than that of the other dyes. All of the dyes' ΔN values are positive as seen in Table 11, demonstrating their ability to donate electrons to iron surfaces and create self-assembling corrosion-inhibiting layers.

Furthermore, the HOMO of all of the dyes is primarily localized on the aromatic rings and azo group, indicating that the aromatic rings and azo group are the preferred sites for an electrophilic attack on metal surfaces, as shown in Figure S11. This implies that the aromatic rings and azo group with high coefficients of HOMO densities are oriented toward the metal surface, and adsorption most likely occurs through the π-electrons of the aromatic rings. Furthermore, the calculations revealed that the charge density of the LUMO level is completely delocalized on the aromatic rings for all of the dyes, implying that the moiety could react as an electrophile (electron acceptor).

Molecular electrostatic potentials (Figure S12) are very useful as the negative regions indicate nucleophilic centers, whereas positive electrostatic potential regions indicate potential electrophilic sites. Furthermore, the electrostatic potential reveals the polarization of the electron density. The calculations revealed that the oxygen atoms of hydroxyl groups have a negative electrostatic potential, indicating that the sites are active centers for metal surface binding.

The synthesized dyes have various active sites for adsorption on metal surfaces. Thus, molecular dynamics calculations were performed on a system containing the dyes and an iron sample to investigate the preferred adsorption site for the interaction between the dyes and the Fe(110) surface. The structures of the adsorbate components were reduced until they met certain criteria. As shown in Table S2, CMBTAP has the highest adsorption energy compared to the other dyes, indicating that the dye has the highest corrosion IE%, which is consistent with the experimental observations. The adsorption energy decreases as the experimental value decreases. E_{ads} decreased in the following order: CMBTAP > CBAMP > CBAN.

The binding energy ($E_{bind} = -E_{ads}$) is the negative of the adsorption energy.[72] The binding energies of all of the dyes are very high. The higher binding energy, the easier adsorption of the dye on metal surfaces, and the greater IE. The binding energy of the synthesized dyes decreases in the following order: CMBTAP > CBAMP > CBAN, and CMBTAP + I^- > CBAMP + I^- > CBAN + I^-, which is consistent with the experimental results. Figures 10 and 11 depict the best adsorption configuration between the dyes and the Fe(110) surface. All of the dyes were adsorbed on the Fe surface through the π-charge of aromatic rings.

The large negative adsorption energies of all of the adsorption systems indicate that the dyes are quickly and tightly adsorbed on the Fe(110) surface. The adsorption energies of the tested dyes are in the order CMBTAP + I^- > CMBTAP > I^-; CBAMP + I^- > I^- > CBAMP, and CBAN + I^- > I^- > CBAN. This trend is consistent with the IE% of CMBTAP.

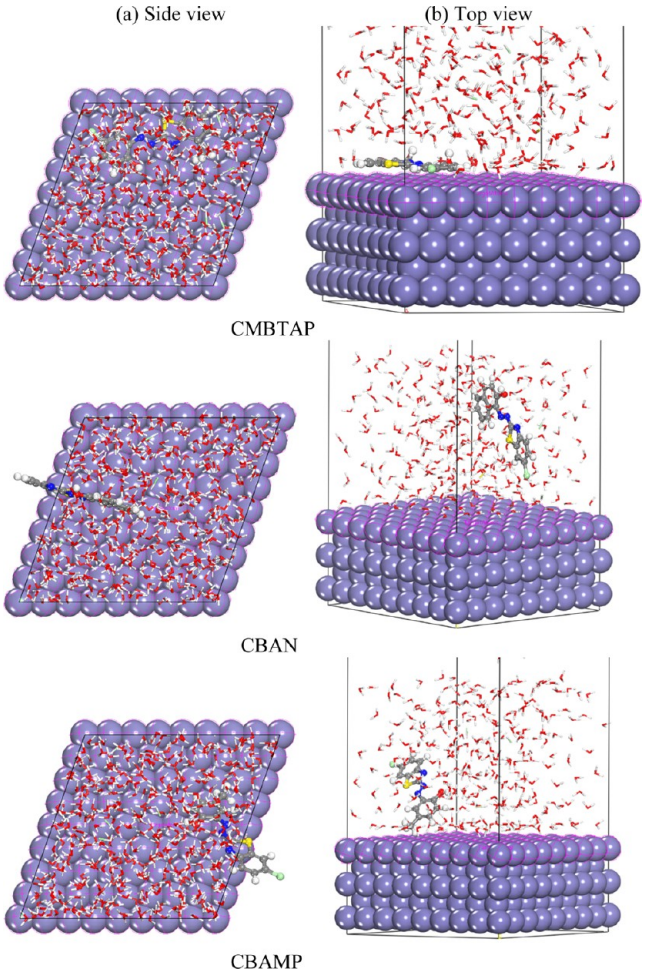

Figure 10. Molecular simulations for the most favorable modes of adsorption obtained for CMBTAP, CBAN, and CBAMP inhibitors on the Fe(110) surface: (a) side view and (b) top view.

4. CONCLUSIONS

Herein, we synthesized novel benzothiazole dyes, including CMBTAP, CBAN, and CBAMP, and characterized them by FT-IR, ^{1}H NMR, ^{13}C NMR, and mass spectroscopy. The corrosion inhibition of the dyes and their synergistic effect with KI on carbon steel in a 1.0 M HCl solution were analyzed through weight loss, electrochemical impedance spectroscopy (EIS), and potentiodynamic polarization measurements. The inhibition efficiency (IE%) was increased with the concentration of the dyes (1×10^{-5}– 2×10^{-4} M) and decreased as the temperature increased from 25 to 45 °C. With the addition of KI to a 1.0 M HCl solution containing the dyes, the corrosion inhibition performance was significantly improved, confirming the synergism between the azo dyes and KI. Potentiodynamic measurements showed that the dyes act as mixed-type

https://doi.org/10.1021/acsomega.3c02105
ACS Omega 2023, 8, 28314−28332

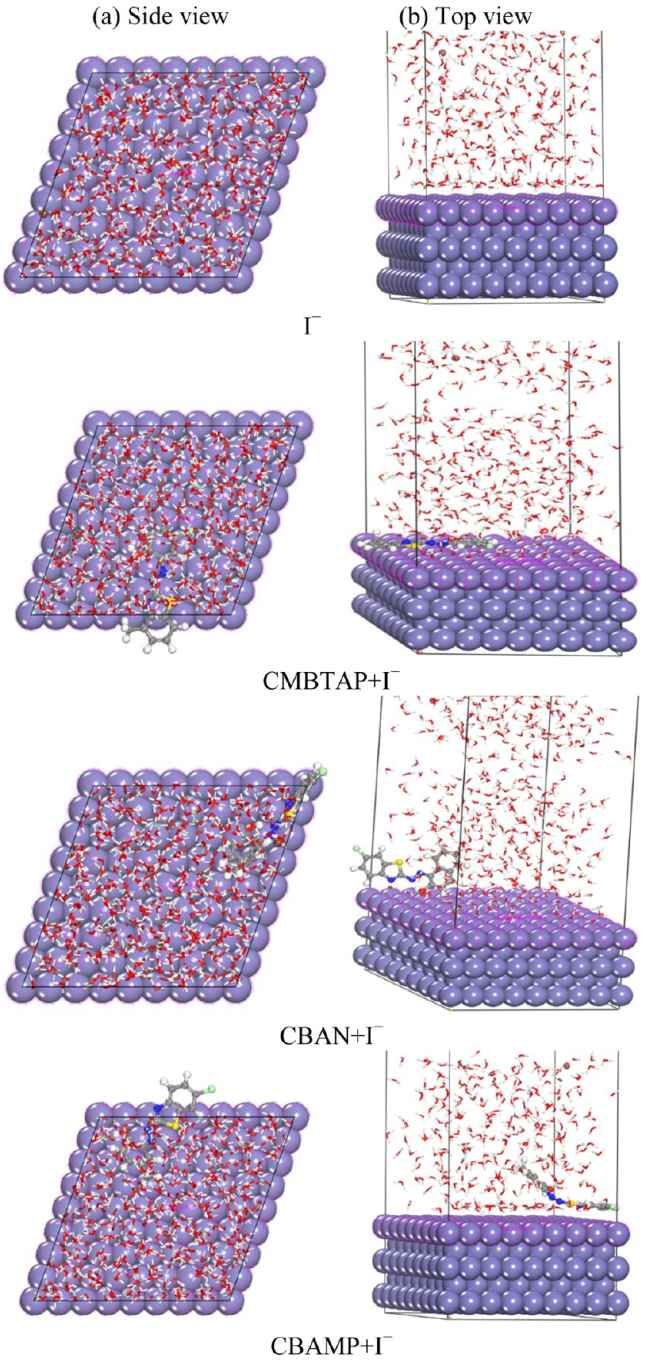

Figure 11. Molecular simulations for the most favorable modes of adsorption obtained for I^-, CMBTAP + I^-, CBAN + I^-, and CBAMP + I^- inhibitors on the Fe(110) surface: (a) side view and (b) top view.

inhibitors. EIS results show that with the addition of the dyes in the HCl solution, the charge-transfer resistance (R_{ct}) increased, which is attributed to the adsorption of the dye molecules on the steel surface. The adsorption of the dyes on the carbon steel surface at different temperatures follows the Langmuir adsorption isotherm, which indicates that the adsorption occurs by chemisorption. SEM, AFM, and EDX analyses were carried out to study the surface morphology and elemental composition on the carbon steel surface in the absence and presence of the inhibitors in 1.0 M HCl solution. The results indicated the effective adsorption of the dye molecules on the surface of carbon steel. Quantum theory calculations evaluated the relationship between the inhibitory efficacy of dyes and their molecular parameters, which confirmed the experimental results. The calculations revealed that the dyes have low energy gap and Milliken and Fukui indices. Among all of the dyes, CMBTAP showed the highest adsorption energy. The corrosion IE was in the order CMBTAP > CBAMP > CBAN.

■ ASSOCIATED CONTENT

Data Availability Statement

All data generated or analyzed during this study are included in this published article.

Supporting Information

The Supporting Information is available free of charge at https://pubs.acs.org/doi/10.1021/acsomega.3c02105.

FT-IR spectra of the investigated CMPTAP; mass spectrum; ^{1}H NMR spectrum; ^{13}C NMR spectrum; $\log K_{ads}$ vs $(1/T)$ curves for carbon steel dissolution; Arrhenius plots for carbon steel corrosion rates (k_{corr}); plots of ($\log k_{corr}$) vs $1/T$ for the corrosion of C-steel; Bode plots for the corrosion of C-steel; equivalent-circuit model used; optimized molecular structures; highest occupied molecular orbital and lowest unoccupied molecular orbital; molecular electrostatic potentials of optimized structures; synergism parameter (S_θ); and outputs and descriptors calculated by the Monte Carlo simulation (PDF)

■ AUTHOR INFORMATION

Corresponding Authors

Mahmoud M. Youssif − *Department of Chemistry, Faculty of Science, Tanta University, Tanta 31527, Egypt*; Email: mahmoudyoussif14@yahoo.com, mahmoud.youssif@science.tanta.edu.eg

Marwa N. El-Nahass − *Department of Chemistry, Faculty of Science, Tanta University, Tanta 31527, Egypt*; orcid.org/0000-0002-7464-404X; Email: marwa.elnahas@science.tanta.edu.eg

Authors

Tarek A. Fayed − *Department of Chemistry, Faculty of Science, Tanta University, Tanta 31527, Egypt*

Hosny A. El-Daly − *Department of Chemistry, Faculty of Science, Tanta University, Tanta 31527, Egypt*

Mohammed M. El-Gamil − *Department of Toxic and Narcotic Drug, Forensic Medicine, Mansoura Laboratory, Medico Legal Organization, Ministry of Justice, Mansoura 35516, Egypt*

Ahmed M. Eldesoky − *Chemical Engineering Department, High Institute of Engineering & Technology, New Damietta 34517, Egypt; Department of Chemistry, University College in Al-Qunfudhah, Umm Al-Qura University, Al-Qunfudhah 21912, Kingdom of Saudi Arabia*

Complete contact information is available at: https://pubs.acs.org/10.1021/acsomega.3c02105

Author Contributions

M.M.Y.: conceptualization, data curation, formal analysis, funding acquisition, investigation, methodology, resources, software, validation, visualization, writing—original draft; M.N.E.-N.: conceptualization, data curation, formal analysis, investigation, resources, software, validation, visualization, writing—review and editing; T.A.F.: conceptualization, data curation, funding acquisition, project administration, super-

https://doi.org/10.1021/acsomega.3c02105
ACS Omega 2023, 8, 28314−28332

vision, writing—review and editing; H.A.E.-D.: supervision; M.M.E.-G.: conceptualization, data curation, formal analysis, software, validation, visualization, writing—review and editing; A.M.E.: formal analysis, data curation, investigation, validation, visualization.

Notes

The authors declare no competing financial interest.

The authors announce that they had active cooperation during the scientific study and preparation of the manuscript. The authors confirm that they have no financial involvement with any commercial company or organization with direct financial interest regarding the materials used in this study. The authors deny any conflicts of interest related to this study.

■ ACKNOWLEDGMENTS

The authors are grateful to the Scientific Research Fund at Tanta University, Egypt, for funding this work through Research Project Code TU:02-19-03.

■ REFERENCES

(1) Haldhar, R.; Prasad, D.; Bahadur, I.; Dagdag, O.; Berisha, A. Evaluation of *Gloriosa superba* seeds extract as corrosion inhibition for low carbon steel in sulfuric acidic medium: A combined experimental and computational studies. *J. Mol. Liq.* **2021**, *323*, No. 114958.

(2) Abhradip, P.; Chandan, D. A novel use of solid waste extract from tea factory as corrosion inhibitor in acidic media on boiler quality steel. *Ind. Crops Prod.* **2020**, *151*, No. 112468.

(3) Hamilton-Amachree, A.; Bartholomew Iroha, N. Corrosion inhibition of API 5L X80 pipeline steel in acidic environment using aqueous extract of *Thevetia peruviana*. *Chem. Int.* **2020**, *6*, 110−121.

(4) Yüce, A. O. Corrosion inhibition behavior of *Robinia pseudoacacia* leaves extract as an eco-friendly inhibitor on mild steel in acidic media. *Met. Mater. Int.* **2020**, *26*, 456−466.

(5) Popoola, L.; Alhaji, S. G.; Ganiyu, K. L.; Babagana, G.; Adebori, S. B. Corrosion problems during oil and gas production and its mitigation. *Int. J. Ind. Chem.* **2013**, *4*, No. 35.

(6) Awad, M. K.; Metwally, M. S.; Soliman, S. A.; El-Zomrawy, A. A.; Bedair, M. A. Experimental and quantum chemical studies of the effect of poly ethylene glycol as corrosion inhibitors of aluminum surface. *J. Ind. Eng. Chem.* **2014**, *20*, 796−808.

(7) Soliman, S. A.; Metwally, M. S.; Selim, S. R.; Bedair, M. A.; Abbas, M. A. Corrosion inhibition and adsorption behavior of new Schiff base surfactant on steel in acidic environment: Experimental and theoretical studies. *J. Ind. Eng. Chem.* **2014**, *20*, 4311−4320.

(8) Ashassi-Sorkhabi, H.; Shabani, B.; Aligholipour, B.; Seifzadeh, D. The effect of some Schiff bases on the corrosion of aluminum in hydrochloric acid solution. *Appl. Surf. Sci.* **2006**, *252*, 4039−4047.

(9) Mallikarjuna, N. M.; Keshavayya, J.; Prasanna, B. M.; Praveen, B. M.; Tandon, H. C. Synthesis, Characterization, and Anti corrosion Behavior of Novel Mono Azo Dyes Derived from 4,5,6,7 Tetrahydro 1,3 benzothiazole for Mild Steel in Acid Solution. *J. Bio- Tribo-Corros.* **2020**, *6*, No. 9.

(10) Fouda, A. S.; Diab, M.; El-Sonbati, A.; Hassan, Sh. A. Benzothiazole derivatives as corrosion inhibitors for carbon steel in 1 M phosphoric acid (H_3PO_4) solutions. *Afr. J. Pure Appl. Chem.* **2013**, *7*, 67−78.

(11) Parameswari, K.; Chitra, S.; Selvaraj, A.; Brindha, S.; Menaga, M. Investigation of Benzothiazole Derivatives as Corrosion Inhibitors for Mild Steel. *Port. Electrochim. Acta* **2012**, *30*, 89−98.

(12) Abboud, Y.; Abourriche, A.; Saffaj, T.; Berrada, M.; Charrouf, M.; Bennamara, A.; Hannache, H. A novel azo dye, 8-quinolinol-5-azoantipyrine as corrosion inhibitor for mild steel in acidic media. *Desalination* **2009**, *237*, 175−189.

(13) Elmorsi, M. A.; Hassanein, A. M. Corrosion inhibition of copper by heterocyclic compounds. *Corros. Sci.* **1999**, *41*, 2337−2352.

(14) Abdallah, M.; Moustafa, E. Inhibition of Acidic Corrosion of Carbon Steel by some Mono and Bis Azo Dyes Based on 1, 5 Dihydroxynaphihalene. *Ann. Chim.* **2004**, *94*, 601−611.

(15) Obot, I. B.; Obi-Egbedi, N. O.; Umoren, S. A. The synergistic inhibitive effect and some quantum chemical parameters of 2,3-diaminonaphtalene and iodide ions on the hydrochloric acid corrosion of aluminum. *Corros. Sci.* **2009**, *51*, 276−282.

(16) Fuchs-Godec, R.; Pavlović, M. G. Pavlovic synergistic effect between non-ionic surfactant and halide ions in the forms of inorganic or organic salts for the corrosion inhibition of stainless-steel X4Cr13 in sulphuric acid. *Corros. Sci.* **2012**, *58*, 192−201.

(17) Mu, G. N.; Li, X. M.; Li, F. Synergistic inhibition between o-phenanthroline and chloride ion on cold rolled steel corrosion in phosphoric acid. *Mater. Chem. Phys.* **2004**, *86*, 59−68.

(18) Li, X.; Deng, S.; Fu, H.; Mu, G. Synergistic inhibition effect of rare earth cerium (IV) ion and sodium oleate on the corrosion of cold rolled steel in phosphoric acid solution. *Corros. Sci.* **2010**, *52*, 1167−1178.

(19) Bedair, M. A. The effect of structure parameters on the corrosion inhibition effect of some heterocyclic nitrogen organic compounds. *J. Mol. Liq.* **2016**, *219*, 128−141.

(20) El-Nahass, M. N.; Fayed, T. A.; El-Daly, H. A.; Youssif, M. M. Benzothiazole azo derivatives as colorimetric probes for optical recognition of different metal ions and anions. *Appl. Organomet. Chem.* **2022**, *36*, No. e6703.

(21) *Modeling and Simulation Solutions for Chemicals and Materials Research, BIOVIA Materials Studio*, version 20.1, accelrys software Inc.: san diego, USA, 2020.

(22) Delley, B. Density functional theory electronic structure program. *J. Chem. Phys.* **2000**, *113*, 7756−7764.

(23) Todorova, T.; Delley, B. Wetting of paracetamol surfaces studied by $DMol^3$-COSMO calculations. *Mol. Simul.* **2008**, *34*, 1013−1017.

(24) Barriga, J.; Coto, B.; Fernandez, B. Molecular dynamics study of optimal packing structure of OTS self-assembled monolayers on SiO_2 surfaces. *Tribol. Int.* **2007**, *40*, 960−966.

(25) Satoh, S.; Fujimoto, H.; Kobayashi, H. Theoretical study of NH_3 adsorption on Fe(110) and Fe(111) surfaces. *J. Phys. Chem. B* **2006**, *110*, 4846−4852.

(26) Guo, L.; Zhu, S.; Zhang, S.; He, Q.; Li, W. Theoretical studies of three triazole derivatives as corrosion inhibitors for mild steel in acidic medium. *Corros. Sci.* **2014**, *87*, 366−375.

(27) Sun, H.; Ren, P.; Fried, J. R. The compass force field: parameterization and validation for phosphazenes. *Comput. Theor. Polym. Sci.* **1998**, *8*, 229−246.

(28) Abdallah, M. Antibacterial drugs as corrosion inhibitors for corrosion of aluminium in hydrochloric solution. *Corros. Sci.* **2004**, *46*, 1981−1996.

(29) Langmuir, I. The constitution and fundamental properties of solids and liquids. *J. Am. Chem. Soc.* **1917**, *39*, No. 1848.

(30) Bhat, J. I.; Alva, V. D. P. Inhibition effect of nevirapine an antiretroviral on the corrosion of mild steel under acidic condition. *J. Korean Chem. Soc.* **2011**, *55*, 835−841.

(31) Oguzie, E. E.; Okolue, B. N.; Ebenso, E. E.; Onuoha, G. M.; Onuchukwu, A. I. Evaluation of the inhibitory effect of methylene blue dye on the corrosion of aluminium in hydrochloric acid. *Mater. Chem. Phys.* **2004**, *87*, 394−401.

(32) Popova, A.; Sokolova, E.; Raicheva, S.; Chritov, M. AC and DC study of the temperature effect on mild steel corrosion in acid media in the presence of benzimidazole derivatives. *Corros. Sci.* **2003**, *45*, 33−58.

(33) Szklarska-Smialowska, Z.; Mankovwski, J. Crevice corrosion of stainless steels in sodium chloride solution. *Corros. Sci.* **1978**, *18*, 953−960.

(34) Yurt, A.; Ulutas, S.; Dal, H. Electrochemical and theoretical investigation on the corrosion of aluminium in acidic solution containing some Schiff bases. *Appl. Surf. Sci.* **2006**, *253*, 919−925.

(35) Zhao, T.; Guannan, Mu. The adsorption and corrosion inhibition of anion surfactants on aluminium surface in hydrochloric acid. *Corros. Sci.* **1999**, *41*, 1937−1944.

https://doi.org/10.1021/acsomega.3c02105
ACS Omega 2023, 8, 28314−28332

(36) Döner, A.; Gülfeza, K. N-Aminorhodanine as an effective corrosion inhibitor for mild steel in 0.5 M H_2SO_4. *Corros. Sci.* **2011**, *53*, 4223−4232.
(37) Ateya, B. G.; El-Anadouli, B. E.; El-Nizamy, F. M. The adsorption of thiourea on mild steel. *Corros. Sci.* **1984**, *24*, 509−515.
(38) Li, X.; Shuduan, D.; Hui, F.; Guannan, M. Synergistic inhibition effect of rare earth cerium (IV) ion and sodium oleate on the corrosion of cold rolled steel in phosphoric acid solution. *Corros. Sci.* **2010**, *52*, 1167−1178.
(39) Li, L.; Xueping, Z.; Jinglei, L.; Jianxin, H.; Shengtao, Z.; Fusheng, P. Adsorption and corrosion inhibition of Osmanthus fragran leaves extract on carbon steel. *Corros. Sci.* **2012**, *63*, 82−90.
(40) Bochris, J. O. M.; Reddy, A. K. N. *Modern Electrochemistry*; Plenum Press: New York, 1970.
(41) Martinez, S.; Stern, I. Thermodynamic characterization of metal dissolution and inhibitor adsorption processes in the low carbon steel/mimosa tannin/sulfuric acid system. *Appl. Surf. Sci.* **2002**, *199*, 83−89.
(42) Tebbji, K.; Bouabdellah, I.; Aouniti, A.; Hammouti, B.; Oudda, H.; Benkaddour, M.; Ramdani, A. N-benzyl-N, N-bis[(3,5-dimethyl-1H-pyrazol-1-yl) methyl] amine as corrosion inhibitor of steel in 1 M HCl. *Mater. Lett.* **2007**, *61*, 799−804.
(43) Mihit, M.; El-Issami, S.; Bouklah, M.; Bazzi, L.; Hammouti, B.; Addi, E. A.; Salghi, R.; Kertit, S. The inhibited effect of some tetrazolic compounds towards the corrosion of brass in nitric acid solution. *Appl. Surf. Sci.* **2006**, *252*, 2389−2395.
(44) Bouklah, M.; Benchat, N.; Hammouti, B.; Aouniti, A.; Kertit, S. Thermodynamic characterisation of steel corrosion and inhibitor adsorption of pyridazine compounds in 0.5 M H_2SO_4. *Mater. Lett.* **2006**, *60*, 1901−1905.
(45) El-Rehim, S. S. A.; Ibrahim, M. A. M.; Khaled, K. F. 4-Aminoantipyrine as an inhibitor of mild steel corrosion in HCl solution. *J. Appl. Electrochem.* **1999**, *29*, 593−599.
(46) Abdallah, M. Ethoxylated fatty alcohols as corrosion inhibitors for dissolution of zinc in hydrochloric acid. *Corros. Sci.* **2003**, *45*, 2705−2716.
(47) Shalabi, K.; Abdallah, Y. M.; Hassan, H. M.; Fouda, A. S. Adsorption and Corrosion Inhibition of Atropa Belladonna Extract on Carbon Steel in 1 M HCl Solution. *Int. J. Electrochem. Sci.* **2014**, *9*, 1468−1487.
(48) Li, L.; Xueping, Z.; Jinglei, L.; Jianxin, H.; Shengtao, Z.; Fusheng, P. Adsorption and corrosion inhibition of Osmanthus fragran leaves extract on carbon steel. *Corros. Sci.* **2012**, *63*, 82−90.
(49) Ferreira, E. S.; Giacomelli, C.; Giacomelli, F. C.; Spinelli, A. Evaluation of the inhibitor effect of l-ascorbic acid on the corrosion of mild steel. *Mater. Chem. Phys.* **2004**, *83*, 129−134.
(50) Tao, Z. H.; Zhang, S. T.; Li, W. H.; Hou, B. R. Corrosion inhibition of mild steel in acidic solution by some oxo-triazole derivatives. *Corros. Sci.* **2009**, *51*, 2588−25950.
(51) Behpour, M.; Ghoreishi, S. M.; Mohammadi, N.; Soltani, N.; Salavati-Niasari, M. Investigation of some Schiff base compounds containing disulfide bond as HCl corrosion inhibitors for mild steel. *Corros. Sci.* **2010**, *52*, 4046−4057.
(52) Larabi, L.; Harek, Y.; Traianel, M.; Mansri, A. Synergistic Influence of Poly(4-Vinylpyridine) and Potassium Iodide on Inhibition of Corrosion of Mild Steel in 1M HCl. *J. Appl. Electrochem.* **2004**, *34*, 833−839.
(53) Lebrini, M.; Lagrenee, M.; Vezin, H.; Traisnel, M.; Bentiss, F. Experimental and theoretical study for corrosion inhibition of mild steel in normal hydrochloric acid solution by some new macrocyclic polyether compounds. *Corros. Sci.* **2007**, *49*, 2254−2269.
(54) Al-Bonayan, A. M. Sodium aliginate as corrosion inhibitor for carbon steel in 0.5 M HCl Solutions. Inter. *J. Sci. Eng. Res.* **2014**, *5*, 611−618.
(55) El-Haddad, M. N.; Fouda, A. S. Corrosion Inhibition and Adsorption Behavior of Some Azo Dye Derivatives on Carbon Steel in Acidic Medium: Synergistic Effect of Halide Ions. *Chem. Eng. Commun.* **2013**, *200*, 1366−1374.
(56) Trinstancho-Reyes, J. L.; Sanchez-Carrillo, M.; Sandoval-Jabalera, R.; Orozco-Carmona, V. M.; Almeraya-Calderon, F.; Chacon-Nava, J. G.; Gonzalez-Rodriguez, J. G.; Martínez-Villafane, A. Electrochemical impedance spectroscopy investigation of alloy inconel 718 in molten salts at high temperature. *Int. J. Electrochem. Sci.* **2011**, *6*, 419−431.
(57) Umoren, S. A.; Ogbobe, O.; Igwe, I. O.; Ebenso, E. E. Inhibition of mild steel corrosion in acidic medium using synthetic and naturally occurring polymers and synergistic halide additives. *Corros. Sci.* **2008**, *50*, 1998−2006.
(58) Umoren, S. A.; Li, Y.; Wang, F. H. Synergistic effect of iodide ion and polyacrylic acid on corrosion inhibition of iron in H_2SO_4 investigated by electrochemical techniques. *Corros. Sci.* **2010**, *52*, 2422−2429.
(59) Zhang, D. Q.; Gao, L. X.; Zhou, G. D. Synergistic effect of 2-mercapto benzimidazole and KI on copper corrosion inhibition in aerated sulfuric acid solution. *J. Appl. Electrochem.* **2003**, *33*, 361−366.
(60) Qu, Q.; Hao, Z.; Jiang, S.; Li, L.; Bai, W. Synergistic inhibition between dodecylamine and potassium iodide on the corrosion of cold rolled steel in 0.1 M phosphoric acid. *Mater. Corros.* **2008**, *59*, 883−888.
(61) Aramaki, K.; Hackerman, N. Inhibition mechanism of medium-sized polymethyleneimine. *J. Electrochem. Soc.* **1969**, *116*, 568−574.
(62) Hassan, H. H. Inhibition of mild steel corrosion in hydrochloric acid solution by triazole derivatives: Time and temperature effects and thermodynamic treatments. *Electrochim. Acta* **2007**, *53*, 1722−1730.
(63) Sastri, V. S.; Perumareddi, J. R. Molecular orbital theoretical studies of some organic corrosion inhibitors. *Corrosion* **1997**, *53*, 617−622.
(64) El-Nahass, M. N.; Bakr, E. A.; El-Gamil, M. M.; Ibrahim, S. A. Synthesis, characterization, and multifunctional applications of novel metal complexes based on thiazolylazo dye. *Appl. Organomet. Chem.* **2022**, *36*, No. e6652.
(65) El-Nahass, M. N.; Fayed, T. A.; Elazim, S. A.; El-Gamil, M. M.; Draz, D. F.; Hassan, F. Multi-sensing response, molecular docking, and anticancer activity of donor−acceptor chalcone containing phenanthrene and thiophene moieties. *J. Mol. Struct.* **2021**, *1240*, No. 130581.
(66) Guo, L.; Ye, G.; Obot, I. B.; Li, X.; Shen, X.; Shi, W.; Zheng, X. Synergistic effect of potassium iodide with L-tryptophane on the corrosion inhibition of mild steel: a combined electrochemical and theoretical study. *Int. J. Electrochem. Sci.* **2017**, *12*, 166−177.
(67) Lalitha, A.; Ramesh, S.; Rajeswari, S. Surface protection of copper in acid medium by azoles and surfactants. *Electrochim. Acta* **2005**, *51*, 47−55.
(68) Awad, M. K.; Issa, R. M.; Atlam, F. M. Theoretical investigation of the inhibition of corrosion by some triazole Schiff bases. *Mater. Corros.* **2009**, *60*, 813−819.
(69) Zhang, D.-q.; Gao, Lx.; Zhou, Gd. Inhibition of copper corrosion in aerated hydrochloric acid solution by heterocyclic compounds containing a mercapto group. *Corros. Sci.* **2004**, *46*, 3031−3040.
(70) Gao, G.; Liang, C. Electrochemical and DFT studies of β-amino-alcohols as corrosion inhibitors for brass. *Electrochim. Acta* **2007**, *52*, 4554−4559.
(71) Lukovits, I.; Kalman, E.; Zucchi, F. Corrosion inhibitors-correlation between electronic structure and efficiency. *Corrosion* **2001**, *57*, 3−8.
(72) Xia, S.; Qiu, M.; Yu, L.; Liu, F.; Zhao, H. Molecular dynamics and density functional theory study on relationship between structure of imidazoline derivatives and inhibition performance. *Corros. Sci.* **2008**, *50*, 2021−2029.

https://doi.org/10.1021/acsomega.3c02105
ACS Omega 2023, 8, 28314−28332